Plant Physiology and Biochemistry 241 (2026) 111988

Contents lists available at ScienceDirect

Plant Physiology and Biochemistry

journal homepage: www.elsevier.com/locate/plaphy

Integrative characterization of two novel *Methylobacterium* species from Argentina expands the diversity of plant-associated methylotrophs

Cecilia Eugenia María Grossi [a], Allison Renee Megow [b], Edgar Martínez-Moyano [a], Md. Asif Mahamud [b], Julieta Mariana Covelli [c], Takakazu Matsuura [b], Akio Tani [b], Nurettin Sahin [d], Rita María Ulloa [a,e,*]

[a] *Laboratorio de Transducción de Señales en Plantas, Instituto de Investigaciones en Ingeniería Genética y Biología Molecular (INGEBI), Consejo Nacional de Investigaciones Científicas y Técnicas (CONICET), Ciudad Autónoma de Buenos Aires, Argentina*
[b] *Institute of Plant Science and Resources, Okayama University, Okayama, Japan*
[c] *Laboratorio de Bioquímica, Microbiología e Interacciones Biológicas en el Suelo, Departamento de Ciencia y Tecnología, Universidad Nacional de Quilmes, Buenos Aires, Argentina*
[d] *Egitim Fakultesi, Mugla Sitki Kocman University, Mentese, Mugla, Turkiye*
[e] *Departamento de Química Biológica, Universidad de Buenos Aires (UBA), Ciudad Autónoma de Buenos Aires, Argentina*

A R T I C L E I N F O

Keywords:
Auxin
Biofilm
Comparative genomics
Methylobacterium
Microbial metabolic profiling
Plant growth-promoting rhizobacteria

A B S T R A C T

Methylobacterium species are facultative methylotrophic bacteria frequently associated with the plant rhizosphere and phyllosphere. Here, the genomic, physiological, and plant-interaction traits of two *Methylobacterium* strains, 1A^T and 2A^T, isolated from potato roots, were compared with those of closely related type species. Phylogenomic analysis based on 107 single-copy core genes placed both strains within group A of the genus *Methylobacterium*. *In silico* DNA-DNA hybridization and average nucleotide identities support their assignment as distinct species. We propose the names *Methylobacterium solani* sp. nov. (type strain 1A^T = RGM 3871^T = DSM 121859^T) and *Methylobacterium torresii* sp. nov. (type strain 2A^T = RGM 3872^T = DSM 121860^T). Comparative pangenomic analysis revealed conserved genes related to plant growth-promoting traits, methylotrophy, as well as strain-specific features such as heavy metal resistance clusters and genomic islands. An integrative approach incorporating phenotypic and metabolic analyses further revealed strain-specific physiological traits, including variation in optimum growth conditions, and carbon utilization. Methylotrophic growth assays revealed distinct growth phenotypes among closely related species, as evidenced by differences in OD_{600}-based growth and responses to lanthanides. Strains 2A^T and *Mb. guangdongense* reached the highest OD_{600} on methanol, while lanthanides slightly stimulated growth in some species. Strain 2A^T grew with 1-aminocyclopropane-1-carboxylate as the sole nitrogen source, and both strains produced indole-3-acetic acid, formed biofilms, and utilized methanol and ethanol, suggesting traits potentially relevant for plant-associated interactions. Strain 1A^T increased lateral root density in *Arabidopsis thaliana*, and inoculation with strain 1A^T, *Mb. oryzae* and *Mb. longum* was associated with increased hypocotyl length in wheat seedlings, as previously reported for strain 2A^T. These findings highlight the potential relevance of these strains in plant-microbe interactions and provide a basis for future studies assessing their performance under greenhouse and field conditions.

1. Introduction

The genus *Methylobacterium* (family *Methylobacteriaceae*), first proposed by Patt et al. (1976), comprises Gram-stain-negative, facultative methylotrophic bacteria. These organisms are characterized by their ability to utilize single-carbon compounds, such as methanol and methylamine, as sole carbon and energy sources (Chistoserdova et al., 2009). While earlier taxonomic revisions based on 16S rRNA phylogeny suggested splitting the genus into *Methylobacterium* and *Methylorubrum* (Green and Ardley, 2018) (hereafter abbreviated as *Mb.* and *Mr.*, respectively), more recent phylogenomic analyses have demonstrated that *Methylobacterium sensu lato* is monophyletic (Alessa et al., 2021; Leducq et al., 2022). Within *Methylobacterium*, however, four

This article is part of a special issue entitled: SI Chile and Argentina published in Plant Physiology and Biochemistry.

* Corresponding author. Vuelta de Obligado 2490, C1428ADN, Ciudad Autónoma de Buenos Aires, Argentina.
E-mail addresses: rulloa@ingebi-conicet.gov.ar, ulloa.rita@gmail.com (R.M. Ulloa).

https://doi.org/10.1016/j.plaphy.2026.111988
Received 20 June 2026; Received in revised form 10 November 2026; Accepted 18 November 2026
Available online 18 November 2026
0981-9428/© 2026 The Authors. Published by Elsevier Masson SAS. This is an open access article under the CC BY-NC-ND license (http://creativecommons.org/licenses/by-nc-nd/4.0/).

Glossary

ABA	abscisic acid
ACC	1-aminocyclopropane-1-carboxylate
AHL:	N-acyl-homoserine lactone
ANI	average nucleotide identity
AUC	area under the curve
CFU	colony-forming units
CK	cytokinin
dDDH	digital DNA-DNA hybridization
dpi	days post-inoculation
DSM	DSMZ German Collection of Microorganisms and Cell Cultures
GIs	genomic islands
HGT	horizontal gene transfer
IAA	indole-3-acetic acid
iP	isopentenyl adenine
IS	insertion sequences
JA	jasmonic acid
JA-Ile	JA-isoleucine
JCM	Japan Collection of Microorganisms
KCTC	Korean Collection for Type Cultures
Ln	lanthanides
LR	lateral roots
MM	mineral medium
Mb	*Methylobacterium*
Mr	*Methylorubrum*
NBRC	NITE Biological Resource Center
PGP	plant growth-promoting
PGPR	plant growth-promoting rhizobacteria
PR	primary root
QS	quorum-sensing
RGM	CChRGM-Colección Chilena de Recursos Genéticos Microbianos
SA	salicylic acid
Trp:	L-tryptophan
tZ	trans-zeatin
μ_{app}:	apparent maximum specific growth rate

well-supported genomic lineages (groups A, B, C, and D) have been identified. Group C represents the most basal lineage and has been proposed as a potential candidate for future recognition as a separate genus, whereas groups A, B, and D, although genetically diverse, do not currently warrant separation at the genus level (Alleman et al., 2025). Currently, the genus includes 60 validly published species (https://lpsn.dsmz.de/genus/methylobacterium; last accessed April 2026).

Often referred to as pink-pigmented facultative methylotrophs (PPFMs), *Methylobacterium* species are ubiquitous, inhabiting diverse environments ranging from soil, air, and water to anthropogenic settings and even the International Space Station (Bijlani et al., 2021; Zhang et al., 2024). Notably, they are among the most abundant bacterial genera in the plant phyllosphere (Knief et al., 2010). This dominance is largely attributed to their specialized metabolism, which allows them to utilize methanol, a byproduct of pectin demethylation during plant cell wall biosynthesis, as a primary carbon source (Fall and Benson, 1996). Methanol oxidation in these bacteria is governed by a "lanthanide switch," involving two types of methanol dehydrogenases: the calcium-dependent MxaF and the lanthanide-dependent XoxF (Skovran et al., 2019; Tani et al., 2021).

Beyond their metabolic association with plants, some *Methylobacterium* species have been recognized as plant growth-promoting rhizobacteria (PGPR). Their beneficial effects on plant growth may involve multiple mechanisms, including the production of phytohormones such as indole-3-acetic acid (IAA) and cytokinins (CKs), 1-aminocyclopropane-1-carboxylate (ACC) deaminase activity, nitrogen fixation, and phosphate solubilization (Grossi et al., 2025; Palberg et al., 2022). Several species, including *Mb. oryzae*, *Mb. radiotolerans*, and *Mb. tardum*, have been reported to promote crop growth under experimental conditions (Chanratana et al., 2017; Priya et al., 2019).

Methylobacterium sp. 2A is a rhizobacterium isolated from the roots of *Solanum tuberosum* L. cv. Désirée potato plants that exhibited strong plant growth-promoting (PGP) traits and was able to produce IAA. When inoculated onto potato and *Arabidopsis thaliana* plants, it alleviated salt stress and showed biocontrol activity against pathogens in dual confrontation assays (Grossi et al., 2020). Genomic analysis revealed the presence of all genes involved in the indole-3-acetamide (IAM) and indole-3-acetonitrile (IAN) pathways for IAA biosynthesis from L-tryptophan (Trp), which have been previously described in bacteria (Tang et al., 2023). Although strain 2A showed promising plant growth-promoting characteristics, its taxonomic position has not yet been established through chemotaxonomic analyses. Some years later, we isolated a second *Methylobacterium* sp. strain, also from the roots of *in vitro* potato plants that were previously grown in the greenhouse. This strain, designated 1A, likely represents a novel species. Hereafter, strain 2A, previously reported as *Methylobacterium* sp. 2A (Grossi et al., 2020, 2024), and strain 1A are referred to as strains 2A^T and 1A^T, the type strains of the two novel species proposed in this study.

In this study, we performed a comprehensive genomic and biochemical comparison of strains 1A^T and 2A^T with their phylogenetic relatives to support their classification as novel species. In addition, we evaluated their PGP abilities by comparing them with other close members of the genus through phytohormone quantification, ACC utilization, biofilm forming capacity and inoculation assays using *A. thaliana* plantlets as well as barley and wheat seeds. Collectively, these findings position these two strains as potential candidates for the development of microbial inoculants in sustainable agriculture.

2. Materials and methods

2.1. Isolation and identification of strain 1A^T

Bacterial isolation was performed in November 2021 from roots of potato plants (*Solanum tuberosum* L. cv. Désirée) established *in vitro*, previously grown in a greenhouse at the Instituto de Investigaciones en Ingeniería Genética y Biología Molecular (INGEBI-CONICET, Argentina; 34°33′28.0″ S, 58°27′32.0″ W). Root tissues showing visible pink pigmentation were collected, surface-sterilized with 70% ethanol followed by 1% sodium hypochlorite treatment, rinsed several times with sterile distilled water, and plated onto non-selective Luria-Bertani medium without NaCl (LBNS; 10 g/L tryptone and 5 g/L yeast extract; Britania S.A., Buenos Aires, Argentina) solidified with 15 g/L agar (Oxoid, Basingstoke, UK). Since the isolation was not intended to selectively recover any specific microbial group, no selective media, antimycotic compounds, or selective antibiotics were used. Plates were incubated at 28 °C for 4 days. Pink-pigmented colonies with similar morphology were observed. A single representative colony was selected for purification and maintained on Reasoner's 2A (R2A; BD Difco™) agar. The taxonomic identity of the isolate was initially assessed by colony PCR amplification and sequencing of the 16S rRNA gene using the universal bacterial primers 8F (5′-AGAGTTTGATCCTGGCTCAG-3′) and 1492R (5′-GGTTACCTTGTTACGACTT-3′). Based on this analysis, the isolate was designated strain 1A^T.

2.2. Bacterial strains and growth conditions

Reference strains were obtained from the Korean Collection for Type Cultures (KCTC), the NITE Biological Resource Center (NBRC), the Japan Collection of Microorganisms (JCM), and the DSMZ German Collection of Microorganisms and Cell Cultures (DSM). Strain 1A^T, strain 2A^T, *Mb. guangdongense* KCTC 8298^T (=SI9^T), *Mb. phyllostachyos* NBRC 105206^T (=BL47^T), *Mb. radiotolerans* JCM 2831^T (= IAM 12098^T), *Mb. oryzae* DSM 18207^T (=CBMB20^T), *Mb. longum* DSM 23933^T, *Mb. tardum* NBRC 103632^T, and *Mb. brachiatum* NBRC 103629^T were stored at −80 °C in R2A broth containing 20% glycerol. Alternative designations refer to the same type strain deposited in different culture collections; the designation of the culture used in this study is used throughout. Prior to experimental use, the strains were streaked from storage onto R2A agar plates and incubated at 28 °C for 2-3 days. Single colonies were then inoculated into 5 mL R2A broth and cultured at 180 rpm using an orbital incubator shaker (Eppendorf® New Brunswick™ Innova® 44, Hamburg, Germany) for 2 days. Bacterial growth was also evaluated at 28 °C using different culture media: LBNS, potato dextrose agar (PDA; Merck KGaA, Darmstadt, Germany), rye sucrose agar (RSA; Caten and Jinks, 1968), and mineral medium (MM; Alamgir et al., 2015).

2.3. DNA extraction and whole-genome sequencing

Strain 1A^T genomic DNA was extracted from two-day-old liquid cultures grown in R2A broth using the DNeasy UltraClean Microbial Kit (Qiagen, Hilden, Germany). Briefly, 1.8 mL of microbial culture was centrifuged at 10,000 × g for 30 s, the supernatant was discarded, and the sample was centrifuged again at 10,000 × g for 30 s to remove the remaining liquid. DNA extraction was then performed according to the manufacturer's instructions. The genome of strain 1A^T was sequenced, assembled, and annotated by Plasmidsaurus (Eugene, OR, USA) using Oxford Nanopore Technologies (ONT) long reads only; no short-read data were generated for this strain. As part of the provider's pipeline, a preliminary taxonomic assignment of each contig was obtained with Mash v2.3 (Ondov et al., 2016) against a RefSeq reference database, reporting the highest-scoring hit and an identity estimated from shared k-mers. Specific sequencing information is detailed in Supplementary Table S1. Genome completeness and contamination were estimated with CheckM (Parks et al., 2015), as reported in the NCBI assembly reports (Supplementary Table S1). The resulting draft genome of strain 1A^T (7,125,460 bp, G + C content 70.87%) was deposited in GenBank under accession JBYQVE000000000 (RefSeq assembly GCF_058072805.1), where it was annotated with the NCBI Prokaryotic Genome Annotation Pipeline (PGAP; Tatusova et al., 2016). The previously reported genome of strain 2A^T (GenBank accession VUOK00000000; RefSeq assembly GCF_009806555.1) (Grossi et al., 2020) was used for comparative phylogenomic, taxonomic, and functional analyses. Specific sequencing information of strain 2A^T genome is also detailed in Supplementary Table S1. Average nucleotide identity (ANI) and *in silico* DNA-DNA hybridization (dDDH) were calculated for strain 1A^T, strain 2A^T, and all validly published *Methylobacterium* and *Methylorubrum* type strains with publicly available genome sequences. ANI values were calculated using the JSpeciesWS web service (Richter et al., 2015). *In silico* DNA-DNA hybridization (dDDH) was performed using the Genome-to-Genome Distance Calculator (GGDC 2.1; Meier-Kolthoff et al., 2013).

2.4. Phylogenomic inference

The phylogenetic analyses based on 16S rRNA gene sequences were carried out with maximum likelihood using the IQ-TREE v2.4.0 (Minh et al., 2020). Related 16S rRNA sequences used in the phylogenetic analysis were retrieved from RefSeq or GenBank accessions and aligned using the SILVA Incremental Aligner (SINA v1.2.12) tool from the arb-silva website (http://www.arb-silva.de/aligner, Pruesse et al., 2012). The robustness for individual branches was estimated by ultrafast bootstrapping (UFBoot) with 1000 replicates (Hoang et al., 2017). To determine the phylogenomic position of strains 1A^T and 2A^T within the genus, bcgTree (Ankenbrand and Keller, 2016) was used to extract amino acid sequences of 107 single-copy core genes from available genomes. A maximum-likelihood (ML) phylogenetic analysis was performed on the concatenated alignment (34,022 amino acid positions) using IQ-TREE v2.4.0 (Minh et al., 2020). The best-fit substitution model (Q.insect + F + I + G4) was selected using ModelFinder (Kalyaanamoorthy et al., 2017). Branch support was assessed using 1000 ultrafast bootstrap replicates and 1000 SH-aLRT tests. To ensure a comprehensive and up-to-date comparator set representing the current taxonomic diversity of the *Methylobacterium/Methylorubrum* lineage, the analysis included genome sequences from all validly published species with publicly available genomes. This dataset included recently described taxa, such as *Mb. amylolyticum* NEAU 140^T, *Mb. ligniniphilum* NEAU K^T (Zhang et al., 2024), *Mb. nigriterrae* SYSU BS000021^T (Chen et al., 2024), *Mb. flocculans* FF17^T (Gao et al., 2024), *Mb. litchii* SD21^T, *Mr. subtropicum* SB2^T, *Mb. guangdongense* SI9^T (Gao et al., 2025), *Mb. alsaeris* MA0201^T, *Mb. carpenticola* ID0610^T (Yoon et al., 2025), *Mb. oryzisoli* sgz302003^T (Liu et al., 2025), *Mb. endophyticum* sgz302541^T (Jiang et al., 2026) and *Mb. synurae* SyP6R^T (Yu et al., 2026).

A pangenome analysis was performed using the OrthoMCL-based pangenome workflow available in KBase (https://www.kbase.us). A reduced comparator set was selected based on the ANI/dDDH-defined closest phylogenetic relatives of each strain. For strain 1A^T, the analysis included *Mb. oryzae* DSM 18207^T and *Mb. radiotolerans* JCM 2831^T, whereas for strain 2A^T, it included *Mb. guangdongense* KCTC 8298^T and *Mb. phyllostachyos* NBRC 105206^T. Orthologous gene clusters were identified and classified as core, shell, or cloud genes. Venn diagrams illustrating the distribution of shared and species-specific genes were generated.

2.5. Detection and analysis of putative plasmid sequences

In strain 1A^T, putative extrachromosomal replicons were identified by contig circularity and the presence of plasmid replication and partitioning genes. In strain 2A^T (short reads only), plasmid sequences were predicted with plasmidSPAdes (Antipov et al., 2016) on Galaxy Europe (https://usegalaxy.eu) using default parameters and the raw reads as input. Scaffolds predicted as putatively plasmid-associated were extracted and annotated using Prokka (Seemann, 2014) to identify coding sequences and assess their functional composition. Both genomes were also screened with PlasmidFinder (Carattoli et al., 2014).

2.6. Genomic island prediction

Potential genomic islands (GIs) acquired through horizontal gene transfer (HGT) were identified by aligning the genome sequences of strains 1A^T and 2A^T with the complete genome of *Mb. oryzae* DSM 18207^T using IslandViewer 4 (Bertelli et al., 2017), followed by manual curation. *Mb. oryzae* was selected as a reference genome due to its high-quality annotation and previous characterization of GI (Kwak et al., 2014), providing a framework for comparative analysis. IslandViewer 4 integrates four prediction methods; however, Islander predictions are available only for pre-computed genomes, so genomic islands in strains 1A^T and 2A^T were predicted with IslandPick, IslandPath-DIMOB, and SIGI-HMM.

2.7. Physiological and biochemical characterization of methylobacterium species

The comparative phenotypic analyses included strains 1A^T and 2A^T together with the closely related type strains *Mb. radiotolerans* JCM 2831^T, *Mb. oryzae* DSM 18207^T, *Mb. guangdongense* KCTC 8298^T, and *Mb. phyllostachyos* NBRC 105206^T, identified as the closest phylogenetic

relatives based on ANI and dDDH analyses. Two additional Group A type strains, *Mb. longum* DSM 23933^T and *Mb. tardum* NBRC 103632^T, were included as contrasting references for plant-interaction traits: *Mb. tardum* has been reported to promote crop growth (Vijayanand et al., 2021), and both species have been described as high biofilm formers (Park et al., 2020). Although some phenotypic characteristics of strain 2A^T had been previously reported (Grossi et al., 2020), its phenotypic profile was reevaluated in this study under the same experimental conditions applied to all strains included in the comparative analysis.

Colony images were acquired after 3 and 5 days of growth on R2A agar at 28 °C using a Leica EZ4D stereomicroscope (Leica Microsystems, Wetzlar, Germany), and colony diameter was measured using ImageJ software. Cell morphology and motility were examined with a Leica DM 2500 LED microscope (Leica Microsystems, Wetzlar, Germany) with fresh liquid cultures. Gram staining was performed using the standard crystal violet-iodine method.

Growth on solid R2A medium was tested at 24, 30, and 37 °C, allowing direct comparison among the analyzed *Methylobacterium* strains. A catalase slide test was performed and oxidase activity was determined by the oxidation of discs impregnated with N, N-dimethyl-*p*-phenylenediamine oxalate (Britania S.A., Argentina).

To evaluate pH tolerance, R2A broth was adjusted to pH values ranging from 5.0 to 10.0 (in 1-unit increments) prior to sterilization by dropwise addition of 1 M HCl or 1 M NaOH to bulk medium preparations under continuous stirring. Target pH values were verified using a calibrated pH meter (HI 2211, Hanna Instruments, Woonsocket, RI, USA) before autoclaving. The sterilized media were dispensed into lidded flat-bottom polystyrene 96-well plates (200 µL per well; edge wells filled with sterile water and not used) and inoculated with 2 µL of a bacterial culture adjusted to an OD_{600} of 0.05. Plates were incubated at 28 °C with rotary shaking at 300 rpm, and OD_{600} was measured every 12 h using a PowerScan HT microplate reader (DS Pharma Biomedical, Osaka, Japan). Readings of medium-only wells, incubated on the same plates, were subtracted as blanks, and the blank-corrected values were converted to a 1-cm light path using a factor of 3.4, as described by Masuda et al. (2018). The readings of the microplate reader were linear up to an OD_{600} of 1.0 (3.4 with a 1-cm light path). No visible cell aggregation was observed under the culture conditions used. OD_{600} was used as a turbidity-based proxy for biomass; it does not distinguish viable from non-viable cells, is non-linear at high densities and instrument-dependent (Stevenson et al., 2016), and can be affected by cell size, poly-β-hydroxybutyrate content and pigmentation; absorbance of medium components was corrected by blank subtraction. The derived parameters, apparent maximum specific growth rate (μ_{app}, h^{-1}) and area under the curve (AUC, OD_{600}·h), therefore describe changes in turbidity rather than in viable cell number. The μ_{app} was estimated from the slope of $\ln(OD_{600})$ versus time during exponential growth, and AUC was calculated using the trapezoidal rule as $\Sigma[(OD_i + OD_{i+1})/2] \times (t_{i+1} - t_i)$, where OD_i and OD_{i+1} are the OD_{600} values at two consecutive time points (t_i and t_{i+1}). Each condition was tested in three biological replicates per strain, and all strains were analyzed under identical experimental conditions, allowing comparative assessment of growth responses across pH treatments. At the end of the experiment, pH values were re-evaluated using pH indicator strips (universal indicator, pH range 0-14, graduations and accuracy of 1 pH unit; MQuant®, Merck), confirming that no major pH changes occurred during incubation.

Salt tolerance was tested on R2A and LBNS agar plates adjusted to final NaCl concentrations of 0, 0.5, 1.0, and 1.5% (w/v). Plates were incubated at 28 °C for five days, and growth was scored qualitatively as present or absent in triplicate for each condition.

Physiological and biochemical profiles of each strain were assessed using API 20 NE and API 50 CH strips (bioMérieux, France), following the manufacturer's instructions. The strips were incubated at 28 °C and monitored daily for seven days. Only results from the final day were recorded. As these assays are qualitative, reactions were interpreted according to the manufacturer's instructions.

Growth in Dworkin and Foster minimal salts medium (DF; Dworkin and Foster, 1958) with or without ACC (Tokyo Chemical Industry Co., Ltd. (TCI), >97% purity) as the nitrogen source was assessed by measuring OD_{600} every 12 h in 96-well microplates over a 96 h period. OD_{600} readings were processed as described above for the pH assays. Each condition was tested with three biological replicates per strain. Growth curves were generated, and the AUC was calculated for each strain under both DF and DF + ACC conditions.

2.8. Chemotaxonomic and polar lipids analysis

For fatty acid methyl ester (FAME) analysis, strain 1A^T, *Mb. radiotolerans* JCM 2831^T, strain 2A^T, and *Mb. phyllostachyos* NBRC 105206^T were cultured on R2A agar at 28 °C for 5 days under identical conditions to minimize variation associated with culture age and growth stage. Microbial biomass was harvested from independent culture plates (biological replicates) and subjected to the standard protocol described by Sasser (2001), including saponification, methylation, and extraction. FAME extracts were analyzed using an Agilent 6850 gas chromatograph equipped with a flame ionization detector (FID). Chromatographic separation was performed using a phenyl-siloxane column (25 m length, 200 µm internal diameter, 0.33 µm film thickness). The oven temperature program started at 170 °C, increased to 260 °C at 5 °C/min, and then ramped at 40 °C/min to a final temperature of 310 °C. Hydrogen was used as the carrier gas and nitrogen as the make-up gas. Fatty acids were identified based on retention times and Kovats retention indices, calculated relative to reference compounds analyzed under identical chromatographic conditions. Relative abundances (%) were calculated based on peak area normalization. For each strain, analyses were performed using five independent biological replicates (n = 5). Chromatographic peaks were integrated for each replicate, and mean values and standard deviations were calculated. Peaks showing retention time deviations greater than 0.1 min among replicates, relative abundances below 0.5% of the total chromatogram area, or detection in fewer than three biological replicates were excluded from the final analysis. HPLC-grade solvents were obtained from Merck (Darmstadt, Germany).

Strain 2A^T, strain 1A^T, *Mb. guangdongense* KCTC 8298^T, and *Mb. radiotolerans* JCM 2831^T were cultivated on R2A agar supplemented with 0.5% methanol at 28 °C for 72 h. Polar lipids were subsequently extracted and analyzed by two-dimensional thin-layer chromatography (TLC) using ALUGRAM® Xtra SIL G/UV254 plates (Macherey-Nagel, Düren, Germany), following the protocol of Rowe et al. (2000). All analyses were performed using independent biological duplicates to confirm reproducibility of the observed lipid profiles.

2.9. Methylotrophic metabolism evaluation

A 96-well plate format was used following previously established protocols (Masuda et al., 2018). Each well contained 200 µL of MM supplemented with 0.5% methanol, either with 30 µM $LaCl_3$ (Nacalai Tesque, Inc., Kyoto, Japan; 95% purity) (MM methanol + Ln) or without $LaCl_3$ (MM methanol − Ln). Bacterial growth was monitored by measuring OD_{600} every 12 h for a total of 60 h. OD_{600} readings were processed as described in Section 2.7. Growth performance was evaluated using AUC values. In addition, ethanol metabolism was tested on solid MM plates with and without 30 µM $LaCl_3$ (MM ethanol ± $LaCl_3$). Three biological replicates per strain and condition were performed. All samples and controls were processed under identical incubation conditions to minimize potential variability associated with solvent evaporation.

2.10. Quantification of phytohormones produced by bacteria in culture

A single colony of each *Methylobacterium* strain was inoculated into 5 mL of R2A medium supplemented with Trp (1 g/L) and incubated for 5 days at 28 °C and 120 rpm. In addition to the strains described in Section

2.7, *Mb. brachiatum* NBRC 103629^T was included in this analysis because its publicly available genome encodes *iaaM* that is also present in strain 2A^T. The OD_{600} was measured, and colony-forming units (CFU) were determined by serial dilution using the drop plate method (Herigstad et al., 2001) and expressed as CFU/mL. Cultures were then centrifuged, and the supernatants were filtered through 0.2 μm cellulose acetate membrane filters to remove bacterial cells. Non-inoculated R2A medium was used as a negative control. An aliquot of 500 μL of each culture supernatant was mixed with 4 mL of 1% acetic acid in acetonitrile/water (4:1, v/v) containing stable isotope-labelled internal standards: D_2-IAA (20 pg/μL, CDN Isotopes Inc.); D_6-ABA (20 pg/μL), D_2-GA1 (20 pg/μL), D_2-GA4 (20 pg/μL), D_4-SA (200 pg/μL), D_5-tZ (1 pg/μL), D_6-iP (1 pg/μL) (Olchemim s.r.o.); D_2-JA (20 pg/μL), and [$^{13}C_6$]JA-Ile (1 pg/μL) (Tokyo Chemical Industry Co. Ltd.). Samples were incubated at 4 °C for 1 h before analysis. Phytohormones (IAA, CKs [trans-zeatin, tZ, and isopentenyl adenine, iP], salicylic acid [SA], gibberellic acid [GA], jasmonic acid [JA], JA-isoleucine [JA-Ile], and abscisic acid [ABA]) were fractionated by successive solid-phase extraction using Oasis HLB, MCX, and WAX cartridges (1 cc, 30 mg; Waters Corp.), with washing and elution steps performed as described by Grossi et al. (2024). The resulting fractions were then analyzed by liquid chromatography-electrospray ionization tandem mass spectrometry (LC-ESI-MS/MS; Agilent 1260 HPLC equipped with a Zorbax Eclipse XDB-C18 column coupled to a G6410B mass spectrometer). Analyte mass-to-charge (m/z) transitions were adopted from Tsukahara et al. (2015). Total phytohormone production was quantified for each culture and expressed both as absolute production and after normalization to bacterial abundance, using the corresponding CFU/mL values. Absolute production is reported per 5 mL culture and, in addition, as concentration in the culture supernatant (per mL).

2.11. Plant Material and Inoculation with methylobacterium species

In this study, we used *A. thaliana* Columbia (Col-0), wheat (cv. Buck Saeta; Buck Semillas S.A., Bs. As., Argentina), and barley (var. Josefina INTA) seeds. *Arabidopsis thaliana* was selected as a standard plant model in plant biology, given its well-characterized genetics, short life cycle, and suitability for rapid screening, making it a widely used first-step model system in PGPR studies. Wheat and barley were additionally selected as agronomically and economically relevant crops in the region, allowing assessment of the practical applicability of these strains beyond the model system. To ensure sterility, all seeds were surface-disinfected as previously described in Grossi et al. (2024). *A. thaliana* seeds were stratified at 4 °C for two days, germinated under sterile conditions on half-strength Murashige and Skoog medium (½ MS; Murashige and Skoog, 1962), which contains no added NaCl, solidified with 0.8% (w/v) agar, and grown in a controlled environment chamber under a 16-h light photoperiod at 21-23 °C for the indicated periods. One-week-old *A. thaliana* seedlings were inoculated onto the root with 2 μL of a bacterial suspension (0.05 OD_{600} units in 0.85% NaCl, used solely as an application vehicle) of each *Methylobacterium* strain or with sterile saline solution as a control. To verify the relationship between OD_{600} and viable cell number, suspensions of each strain adjusted to an OD_{600} of 0.05 in 0.85% NaCl were plated by serial dilution using the drop plate method (Herigstad et al., 2001) in three independent experiments. These suspensions contained (mean ± SD, n = 3): strain 1A^T, (2.52 ± 0.85) × 10^7 CFU/mL; *Mb. phyllostachyos* NBRC 105206^T, (1.67 ± 0.38) × 10^7 CFU/mL; *Mb. radiotolerans* JCM 2831^T, (2.32 ± 0.40) × 10^7 CFU/mL; *Mb. oryzae* DSM 18207^T, (3.17 ± 1.67) × 10^7 CFU/mL; *Mb. longum* DSM 23933^T, (1.57 ± 0.61) × 10^7 CFU/mL; and *Mb. tardum* NBRC 103632^T, (1.55 ± 0.43) × 10^7 CFU/mL. No significant differences in viable cell concentrations were detected among strains (one-way ANOVA, p = 0.197). At 3 and 5 days post-inoculation (dpi), plants were photographed, and primary root (PR) length (mm) and lateral root (LR) number were quantified using ImageJ software, as previously described by Grossi et al. (2020). LR density was calculated as the number of LR per mm of PR length (LR/mm PR). According to Grossi et al. (2024), three independent plates containing five plants each were analyzed per treatment; each plate was inoculated using a freshly prepared independent bacterial culture.

Monocot seeds were incubated with cell suspensions of *Methylobacterium* strains (0.1 OD_{600} units in 0.85% NaCl) or with sterile 0.85% NaCl (control) on an Orbit™ LS Low Speed Laboratory Shaker (Labnet International, Edison, NJ, USA) at 60 rpm for 30 min. After treatment, seeds were dried on sterile Whatman No. 1 (11 μm) filter paper for 30 min in a laminar flow hood and then placed in humid chambers moistened with sterile distilled water, without added NaCl, for germination. Seeds were exposed to a 3 h pulse of white LED light (1012 lux at seed level), after which germination proceeded in darkness. At 4 dpi, germination was assessed based on visible radicle emergence. Germination rates were 93% for wheat and 72% for barley. Four independent experiments using freshly prepared bacterial cultures were performed on separate days comparing control plates with treated ones. Each plate was independently inoculated and considered an experimental unit. In each experiment, the mean value of each parameter was calculated from 25 seedlings per plate. Values for inoculated plates were normalized to the mean of the non-inoculated control plates from the same experiment. Morphological measurements were performed only on germinated seedlings that had developed both a visible root system and a shoot. Hypocotyl length (cm) and the number of roots per plant were measured in wheat and barley seedlings, and in barley the length of the longest root (cm) was also recorded.

2.12. Biofilm formation and production of N-acyl-homoserine lactones

Biofilm formation was evaluated under static conditions in a 96-well plate, following the method described by O'Toole (2011). The plate was incubated at 28 °C without agitation for 5 days. The liquid was then removed, and adherent biofilm-forming cells on the well surfaces were stained with 0.1% crystal violet solution (w/v) in water. At this stage, images of the well bottoms were captured using the stereomicroscope. For each bacterial treatment four wells were used.

N-acyl-homoserine lactones (AHLs) were detected using two *Chromobacterium violaceum* biosensor strains: CV026 and VIR07. CV026 responds to short-chain AHLs, while VIR07 responds to long-chain AHLs, both through induction of violacein production (Morohoshi et al., 2008). For the assay, LB agar plates were divided into quarters, and each *Methylobacterium* strain was streaked in a designated quarter. After three days of incubation, the biosensor strains were streaked adjacent to the test strains in a "T" formation. A positive result was indicated by a color change in *C. violaceum* from white to violet. As controls, *Pseudomonas aeruginosa* strain PAO1 (positive) and *Escherichia coli* DH5α (negative) were co-cultured with the biosensor strains (Huang et al., 2003; Smith et al., 2011). Plates were incubated at 28 °C for an additional three days. The assay was repeated three times, with two replicates per strain.

2.13. Statistical analysis

Statistical analyses were performed for quantitative experiments according to the experimental design of each assay. One-way or two-way analysis of variance (ANOVA), followed by Tukey's HSD test was used for experiments involving comparisons among multiple groups or factors, as specified in the corresponding figure or table legends. Qualitative assays were not subjected to statistical analysis. Exact p-values are reported in the text for individual comparisons, except where $p < 0.0001$. Figures and tables indicate significant differences with letters or asterisks, as explained in their legends. All statistical analyses and graphs were performed using GraphPad Prism version 8.4.3 (GraphPad Software, La Jolla, CA, USA).

3. Results

3.1. Genomic comparison with closely related type strains places strains 1A^T and 2A^T within group A

16S rRNA gene phylogeny placed strain 1A^T within the cluster containing *Mb. oryzae*, whereas strain 2A^T clustered with *Mb. ligniniphilum* and *Mb. guangdongense* (Supplementary Fig. S1). To further resolve their taxonomic positions, whole-genome analyses were performed. The phylogenomic positions of strain 1A^T and 2A^T within the genus *Methylobacterium* were determined using 76 type strains of established *Methylobacterium* and *Methylorubrum* species (Fig. 1). Both strains were assigned to Group A, which included 34 members. Within this group, strain 2A^T formed a distinct sub-branch alongside *Mb. phyllostachyos* (Madhaiyan and Poonguzhali, 2014) and *Mb. guangdongense* KCTC 8298^T, whereas strain 1A^T clustered with *Mb. radiotolerans*. Strain 1A^T showed 51.6% dDDH with *Mb. radiotolerans*, and 38.7% dDDH with *Mb. oryzae*. Similarly, strain 2A^T exhibited 39.9% dDDH with *Mb. guangdongense* KCTC 8298^T, and 37.0% dDDH with *Mb. phyllostachyos* NBRC 105206^T. These values are well below the accepted thresholds for species delineation (70% for dDDH) supporting their separation from closely-related taxa. ANI analyses performed using JSpecies revealed values of 92.4% between strain 1A^T and *Mb. radiotolerans*, and 88.7% with *Mb. oryzae*. Likewise, strain 2A^T showed ANI values of 88.7% with *Mb. guangdongense* KCTC 8298^T and 87.8% with *Mb. phyllostachyos* NBRC 105206^T. All ANI values were below the accepted 95% threshold, further supporting their classification as distinct species.

3.2. Genomic analysis revealed genes related to plant growth-promoting traits and environmental adaptation in strains 1A^T and 2A^T

A pangenomic comparison of strain 2A^T with *Mb. guangdongense* KCTC 8298^T and *Mb. phyllostachyos* NBRC 105206^T, and of strain 1A^T with *Mb. oryzae* DSM 18207^T and *Mb. radiotolerans* JCM 2831^T, revealed that 2A^T and 1A^T share 3214 and 3398 core gene clusters with their closest relatives, respectively (Supplementary Fig. S2A). Core gene families are usually involved in essential cellular processes required for survival across diverse environmental conditions (Samanta et al., 2024). Conserved genes included an ACC deaminase (*acdS*), the tryptophan biosynthetic cluster (*trpA-G*), *miaA* (tRNA isopentenyltransferase), genes linked to phenazine biosynthesis (*phzF*), penicillin tolerance (*PAH* and *pbpG*), and copper transport (*actP*). These genes are also present in other members of the group such as *Mb. longum* DSM 23933^T and *Mb. tardum* NBRC 103632^T (Supplementary Table S2**)**. All genomes contained *mxbDM*, the *xox* and *pqq* clusters, H_4MPT pathway genes, formaldehyde-activating enzymes, and the Ln^{3+}-dependent alcohol dehydrogenase *exaF* (Supplementary Table S3**)**. Several IAA-related genes (*amiE, nthA, nthB,* and *nit*) were present in most strains; however, *Mb. longum* lacked *amiE* and *nit*. Genes associated with the oxidative stress response were also detected, except for the catalase-peroxidase (*katG*), which was absent in strain 2A^T and in *Mb. tardum*. We identified the complete 15-gene *mxa* cluster, with a conserved organization relative to *Mr. extorquens* AM1, except in *Mb. longum* DSM 23933^T and *Mb. tardum* NBRC 103632^T. Highest sequence identity within the cluster was observed between 2A^T and *Mb. phyllostachyos*, and between 1A^T and *Mb. radiotolerans* **(**Supplementary Table S3; Supplementary Fig. S2B**)**.

Unique gene clusters (cloud genes) in strains 1A^T and 2A^T totaled 275 and 564, respectively, whereas shell genes (shared by two of the three compared strains) comprised 621 and 421 gene clusters, respectively (Supplementary Fig. S2A). Notably, strain 2A^T harbors the *iaaM* gene involved in auxin biosynthesis which is rare within the genus. It is present only in eleven type strains of validly published *Methylobacterium* species from different groups: *Mb. brachiatum*, *Mb. pseudosasicola*, *Mb. mesophilicum*, *Mb. persicinum*, *Mb. thuringiense*, *Mb. organophilum*, *Mb. brachythecii*, *Mb. platani*, *Mb. terrae*, *Mb. bullatum*, and *Mb. iners*.

GIs analysis predicted 26 and 50 islands in strains 2A^T and 1A^T, respectively, representing 8.6% and 11.16% of their genomes. In strain 2A^T, GI22 contains a nodulation protein *nolO* gene showing 69.95% identity to a homolog from *Pirellulales bacterium*, suggesting HGT. In strain 1A^T, GI42 encodes a 14-gene Type VI secretion system (T6SS) within a 19,901 bp region highly similar to *Mb. fujisawaense* C14 (93.87% identity) but absent from other *Methylobacterium* species **(**Supplementary Fig. S3**)**. Thirty-six genes were shared exclusively between strains 1A^T and 2A^T, including *merA* (mercuric reductase) and *merB* (alkylmercury lyase), which confer narrow- and broad-spectrum mercury resistance, respectively (Golysheva et al., 2025). Strain 2A^T harbors a *merTPAB* operon within GI26 and four arsenate resistance genes located in GI17. In contrast, strain 1A^T carries five mercury resistance genes (*merTPFAB*) clustered within GI21 and encodes eleven arsenate resistance genes, six of which are strain-specific (Supplementary Table S2). These *mer* operons show high identity (82.58% and 79.88%, respectively) to plasmid-borne systems present in *Pseudomonas* sp. K-62 that confer resistance to both mercuric ions and organomercurials (Sone et al., 2013).

3.3. Detection of extrachromosomal sequences

The strain 1A^T assembly comprised two linear contigs (4,144,668 and 2,440,289 bp), together forming a 6,584,957-bp chromosome, and a circular 540,503-bp contig (contig_5 in the provider's output). Mash assigned both chromosomal contigs to *Methylobacterium radiotolerans* JCM 2831 (NC_010505.1; 92.5% and 91.5% estimated identity). Contig_5 carried a *repABC* cluster spanning the linearization point, comprising *repC* (539,096–540,433), *repA* (52-1227) and *repB* (1232–2308), together with an additional gene encoding a protein annotated as replication protein RepA (537,816–538,904). A second *repC* copy was located at 415,601–416,731. The G + C content of contig_5 (70.59%) was similar to that of the chromosome (70.89%). Contig_5 showed only a distant Mash hit to the *Mb. oryzae* DSM 18207^T (=CBMB20^T) chromosome (NZ_CP003811.1; Kwak et al., 2014; 77.6% estimated identity), which is consistent with the absence of closely related replicons in the reference database. Together, its circularity and the presence of *repABC* genes suggest that contig_5 is a large plasmid-like replicon. PlasmidFinder detected no replicons in either genome, as expected given that its database lacks alphaproteobacterial *repABC*-type replicons. In strain 2A^T, plasmidSPAdes predicted six putative plasmid scaffolds (63,467 bp in total) but no complete circular plasmid. These scaffolds encoded mainly hypothetical proteins and mobile elements (transposases, insertion sequences, recombinases), along with regulatory proteins, toxin-antitoxin systems and DNA-processing enzymes, but no plasmid replication or maintenance genes.

3.4. Phenotypic characterization of novel strains 1A^T and 2A^T

The genomic information of the novel *Methylobacterium* strains 1A^T and 2A^T, together with their differential phenotypic characteristics compared with related *Methylobacterium* type species, is summarized in Table 1. The majority of the phenotypic characteristics of these strains were similar to those of other *Methylobacterium* species. Both strains were Gram-stain-negative and rod-shaped, consistent with the previous description of strain 2A^T (Grossi et al., 2020). Strain 1A^T was catalase- and oxidase-positive, while catalase and oxidase activities of strain 2A^T had been previously reported (Grossi et al., 2020) and were confirmed here under the same experimental framework. After 3 days of growth on R2A agar, pink-pigmented colonies with diameters of 0.06 mm for 1A^T and 0.20 mm for 2A^T were observed (Table 1; colony morphology after 5 days is shown in Supplementary Fig. S4). Growth on R2A agar was observed between 24 and 30 °C; however, strain 2A^T also showed visible growth at 37 °C. Both strains 1A^T and 2A^T were able to grow on PDA and RSA, confirming previous reports for strain 2A^T (Grossi et al., 2020). Strains 1A^T and 2A^T grew in both R2A and LBNS media containing up to

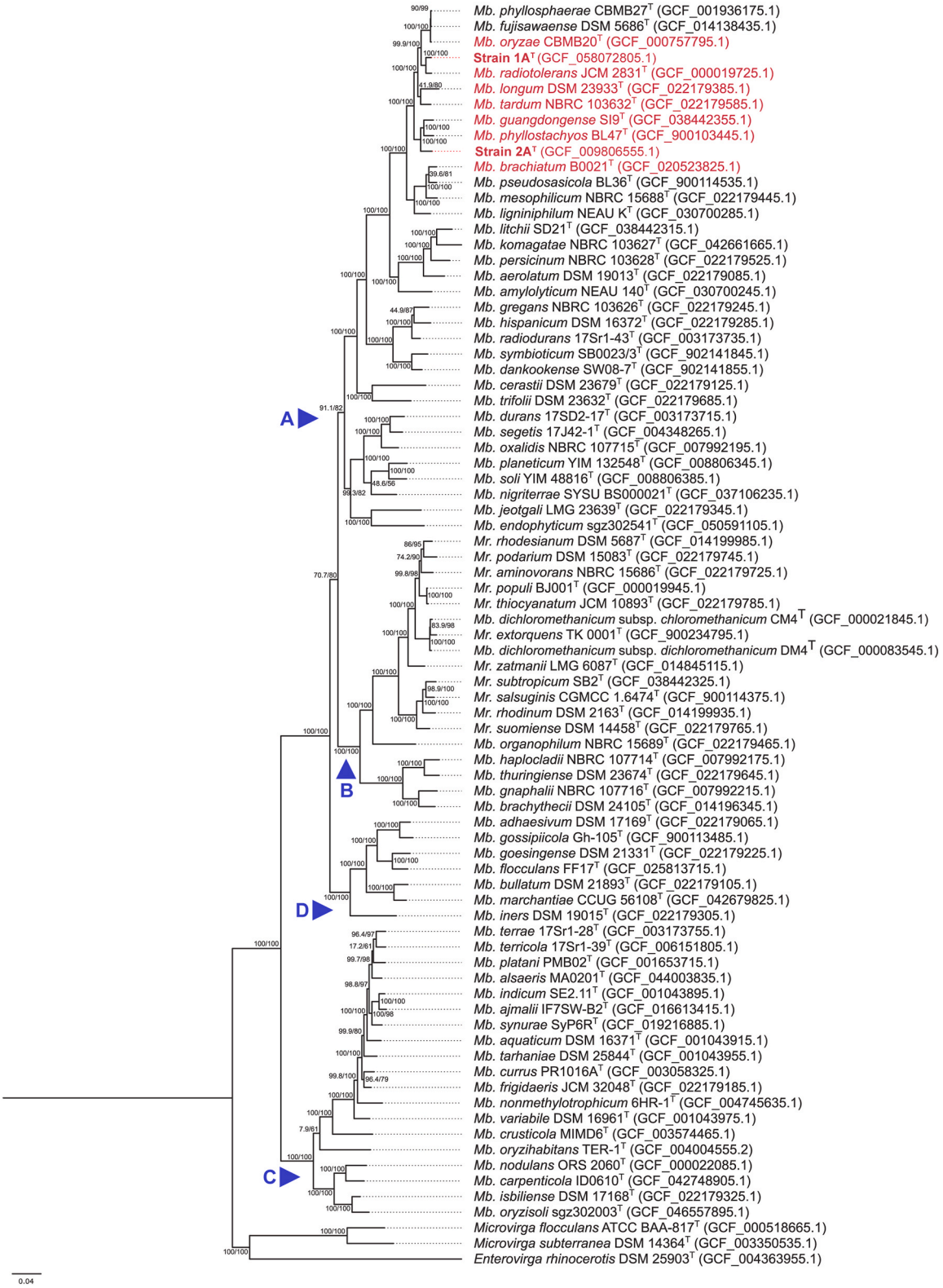

Fig. 1. Phylogenomic tree of strains 1A^T and 2A^T with type strains of *Methylobacterium* (*Mb*) and *Methylorubrum* (*Mr*). The tree was reconstructed based on the concatenated amino acid alignment of 107 single-copy core genes identified with bcgTree. Maximum-likelihood analysis was performed using IQ-TREE 2 under the Q.insect + F + I + G4 substitution model selected by ModelFinder. The final alignment comprised 34,022 amino acid positions. Assembly accession numbers are indicated in parentheses. Strain designations correspond to those of the deposited genome assemblies (e.g., *Mb. guangdongense* SI9^T = KCTC 8298^T, *Mb. phyllostachyos* BL47^T = NBRC 105206^T, *Mb. oryzae* CBMB20^T = DSM, 18207^T). *Microvirga* and *Enterovirga* species were included as outgroups, and the tree was midpoint-rooted. Branch support values are shown as SH-aLRT (%)/bootstrap (%). The scale bar indicates 0.04 substitutions per site. Phylogenetic groups A-D are marked with blue triangles. Species highlighted in red were further analyzed in this study.

Table 1
Genomic and phenotypic characteristics of strains 1A^T (*Mb. solani* sp. nov.) and 2A^T (*Mb. torresii* sp. nov.) and related *Methylobacterium* type strains analyzed in this study. Colony morphology and growth characteristics are shown; API 20 NE and API 50 CH profiles are provided in Supplementary Tables S4 and S5, respectively. Strain designations correspond to the cultures used in this study; alternative designations given in parentheses refer to the same type strain deposited in other culture collections. +, positive; −, negative; N.D., not determined. Gene counts correspond to the NCBI RefSeq annotation of each assembly.

Species	*Mb. solani*	*Mb. radiotolerans*	*Mb. oryzae*	*Mb. torresii*	*Mb. guangdongense*	*Mb. phyllostachyos*	*Mb. longum*	*Mb. tardum*
Strain	1A^T (= RGM 3871^T = DSM 121859^T)	JCM 2831^T (= IAM 12098^T)	DSM 18207^T (=CBMB20^T)	2A^T (= RGM 3872^T = DSM 121860^T)	KCTC 8298^T (=SI9^T = GDMCC 1.14329^T)	NBRC 105206^T (=BL47^T)	DSM 23933^T	NBRC 103632^T
Isolated from	Potato roots	Unhulled old rice	Stem tissue of rice	Potato roots	Phyllosphere of litchi	Bamboo leaf surface	Phyllosphere of *A. thaliana*	Food factory
Genomic data								
Accession number	GCF_058072805.1	GCF_000019725.1	GCF_000757795.1	GCF_009806555.1	GCF_038442355.1	GCF_900103445.1	GCF_022179385.1	GCF_022179585.1
Length (bp)	7,125,460	6,298,400	6,286,629	6,395,352	6,470,023	6,015,046	6,595,241	6,885,325
G + C content (%)	70.87	71.28	69.77	69.5	69.07	68.69	69.33	69.17
Protein-coding genes	6.614	6.449	5.664	5.962	6.179	5.675	6.178	6.445
Growth in different media at 28 °C								
PDA	+	+	+	+	+	+	-	-
RSA	+	+	+	+	N.D.	+	-	+
Growth in R2A								
24 °C	+	+	+	+	+	+	+	+
30 °C	+	+	+	+	+	+	-	+
37 °C	-	+	+	+	-	-	-	+
Colony diameter in R2A (mm)								
3 days of growth	0.06 ± 0.01	0.30 ± 0.05	0.20 ± 0.02	0.20 ± 0.04	0.24 ± 0.04	0.12 ± 0.01	-	0.16 ± 0.02
5 days of growth	0.09 ± 0.00	0.35 ± 0.04	0.22 ± 0.04	0.21 ± 0.04	0.53 ± 0.13	0.12 ± 0.01	0.09 ± 0.01	0.21 ± 0.01
NaCl tolerance (R2A/LBNS)								
0%	+/+	+/+	+/+	+/+	+/+	+/−	+/+	+/+
0.5%	+/+	+/+	+/+	+/+	+/+	+/+	−/−	+/−
1%	−/−	+/+	+/+	−/−	+/−	+/−	−/−	+/−
1.5%	−/−	−/−	−/−	−/−	−/−	−/−	−/−	−/−
Growth in MM ethanol								
with LaCl3	+	+	+	+	+	+	+	-
w/o LaCl3	+	+	+	+	+	+	+	-

0.5% NaCl, with no growth observed at higher concentrations. In comparison, their closest relatives showed greater salt tolerance: *Mb. oryzae* DSM 18207^T and *Mb. radiotolerans* JCM 2831^T grew in both media up to 1% NaCl, while *Mb. guangdongense* KCTC 8298^T and *Mb. phyllostachyos* NBRC 105206^T also grew up to 1% NaCl, but only in R2A medium. *Mb. tardum* NBRC 103632^T likewise grew up to 1% NaCl in R2A medium. In contrast, *Mb. longum* DSM 23933^T only grew in the absence of NaCl and did not tolerate any of the concentrations tested (Table 1).

OD-based growth parameters (AUC and μ_{app}) were determined for each isolate and reference strain across pH 5-10 (Table 2). Overall, strain 1A^T AUC values were significantly lower than *Mb. radiotolerans* JCM 2831^T and *Mb. oryzae* DSM 18207^T across the full pH range, while strain 2A^T displayed marked sensitivity to alkaline conditions, with AUC values significantly lower than *Mb. guangdongense* KCTC 8298^T but significantly higher than *Mb. phyllostachyos* NBRC 105206^T under most conditions tested (except pH 7). These trends were consistent with the apparent growth rate (μ_{app}) values. For strain 1A^T, μ_{app} was significantly lower than *Mb. oryzae* DSM 18207^T at all pH except 8, and than in *Mb. radiotolerans* JCM 2831^T at pH 7, 9, and 10. For strain 2A^T, μ_{app} was significantly lower than *Mb. guangdongense* KCTC 8298^T at pH 7, 9, and 10, with the largest relative difference at pH 9 (0.038 vs. 0.097 h^{-1}, $p < 0.0001$). Relative to *Mb. phyllostachyos* NBRC 105206^T, strain 2A^T showed significantly higher μ_{app} at all pH except 7, with *Mb. phyllostachyos* NBRC 105206^T growth strongly reduced at pH 9-10 (μ_{app} = 0.015-0.018 h^{-1}). Descriptive values for *Mb. longum* DSM 23933^T and *Mb. tardum* NBRC 103632^T are reported in Table 2 but were not statistically compared.

To identify the pH at which each strain reached the highest turbidity-based growth, AUC values were compared across pH conditions within each strain (Supplementary Fig. S5). Strain 1A^T, *Mb. radiotolerans* JCM 2831^T, and *Mb. oryzae* DSM 18207^T displayed the highest AUC at pH 6, with strain 1A^T showing significantly higher AUC at pH 6 than at all other pH values tested ($p < 0.01$-0.0001). In contrast, strain 2A^T and *Mb. guangdongense* KCTC 8298^T showed the highest AUC at pH 5, with AUC declining progressively as pH increased; this decline was most pronounced for strain 2A^T, which showed a significant drop at pH 9-10 vs. pH 5-8 ($p < 0.0001$). *Mb. phyllostachyos* NBRC 105206^T showed the highest AUC at pH 6, with growth strongly reduced at pH 9-10 vs. pH 5-8 ($p < 0.0001$). *Mb. longum* DSM 23933^T showed no significant differences in AUC across pH 6-10, but growth at pH 5 was markedly impaired relative to all other conditions ($p < 0.0001$). *Mb. tardum* NBRC 103632^T showed no clear pH-dependent pattern.

The complete phenotypic profiles obtained using API 20 NE and API 50 CH strips are presented in Supplementary Tables S4 and S5, respectively. Strain 1A^T, *Mb. radiotolerans* JCM 2831^T, and *Mb. oryzae* DSM 18207^T assimilated potassium gluconate, adipic acid, and malic acid. However, strain 1A^T exhibited urease activity but did not reduce nitrate, whereas *Mb. radiotolerans* JCM 2831^T and *Mb. oryzae* DSM 18207^T reduced nitrate but lacked urease activity. On the other hand, strain 2A^T and *Mb. guangdongense* KCTC 8298^T were negative for glucose fermentation but positive for arginine hydrolysis, while *Mb. phyllostachyos* NBRC 105206^T showed the opposite pattern. All three strains were urease-positive. Assimilation profiles further differentiated them: strain 2A^T preferentially utilized L-arabinose and potassium gluconate; *Mb. guangdongense* KCTC 8298^T grew best on glucose, D-mannitol, N-acetyl-glucosamine, D-maltose, potassium gluconate and adipic acid; and *Mb. phyllostachyos* NBRC 105206^T preferentially assimilated potassium gluconate and adipic acid. *Mb. longum* DSM 23933^T and *Mb. tardum* NBRC 103632^T displayed identical API 20 NE profiles, with no detectable carbon assimilation and enzymatic activity limited to urease and glucose fermentation (Supplementary Table S4). In the API 50 CH strips, strains 1A^T and 2A^T exhibited carbohydrate utilization profiles distinct from those of related species (Supplementary Table S5). Strain 1A^T strongly assimilated glycerol and potassium gluconate, and weakly assimilated D-arabinose, D-glucose and D-lyxose. Strain 2A^T showed a broader substrate range, with strong utilization of glycerol, D-fructose, D-lyxose,

Table 2
Growth parameters of *Methylobacterium* strains at different pH conditions. The apparent maximum specific growth rate (μ_{app}, h^{-1}) and the area under the growth curve (AUC, OD_{600}·h) were determined for each strain grown at pH 5, 6, 7, 8, 9, and 10. Data are mean ± SD (n = 3). Statistical comparisons were performed independently at each pH using one-way ANOVA followed by Tukey's multiple comparisons test, between each novel strain and its closest phylogenetic relatives: strain 1A^T vs. *Mb. radiotolerans* and vs. *Mb. oryzae*; strain 2A^T vs. *Mb. guangdongense* and vs. *Mb. phyllostachyos*. ns, not significant ($p \geq 0.05$); *$p < 0.05$, **$p < 0.01$, ***$p < 0.001$, ****$p < 0.0001$. *Mb. longum* and *Mb. tardum*, included as contrasting Group A references for plant-interaction traits, are shown for descriptive purposes only and were not statistically compared.

	Strain 1A^T	*Mb. radiotolerans* JCM 2831^T	*Mb. oryzae* DSM 18207^T	Strain 2A^T	*Mb. guangdongense* KCTC 8298^T	*Mb. phyllostachyos* NBRC 105206^T	*Mb. longum* DSM 23933^T	*Mb. tardum* NBRC 103632^T
μ_{app} (h^{-1})								
pH 5	0.112 ± 0.006	0.134 ± 0.012 ns	0.165 ± 0.014 **	0.110 ± 0.012	0.136 ± 0.013 ns	0.067 ± 0.009 **	0.021 ± 0.004	0.129 ± 0.011
pH 6	0.145 ± 0.009	0.152 ± 0.010 ns	0.182 ± 0.012 **	0.102 ± 0.011	0.124 ± 0.012 ns	0.074 ± 0.008 *	0.098 ± 0.009	0.143 ± 0.012
pH 7	0.104 ± 0.008	0.129 ± 0.009 *	0.158 ± 0.010 ***	0.085 ± 0.010	0.118 ± 0.011 **	0.070 ± 0.006 ns	0.107 ± 0.008	0.118 ± 0.010
pH 8	0.118 ± 0.011	0.138 ± 0.013 ns	0.141 ± 0.012 ns	0.092 ± 0.011	0.109 ± 0.010 ns	0.049 ± 0.007 **	0.112 ± 0.010	0.124 ± 0.011
pH 9	0.095 ± 0.010	0.121 ± 0.011 *	0.128 ± 0.011 *	0.038 ± 0.006	0.097 ± 0.009 ****	0.018 ± 0.004 *	0.101 ± 0.009	0.116 ± 0.010
pH 10	0.083 ± 0.007	0.109 ± 0.009 *	0.119 ± 0.010 **	0.041 ± 0.007	0.083 ± 0.008 ***	0.015 ± 0.005 **	0.095 ± 0.008	0.104 ± 0.009
AUC (OD_{600}·h)								
pH 5	24.96 ± 1.02	33.75 ± 1.82 **	42.38 ± 2.30 ****	22.77 ± 1.08	28.67 ± 1.33 **	13.72 ± 1.52 ***	2.12 ± 0.09	28.46 ± 1.64
pH 6	30.88 ± 1.41	35.92 ± 2.01 *	48.11 ± 2.54 ****	20.95 ± 0.97	26.03 ± 1.19 **	16.84 ± 0.91 **	22.84 ± 1.33	31.92 ± 1.77
pH 7	22.41 ± 1.26	29.74 ± 1.63 **	44.20 ± 2.12 ****	17.62 ± 0.84	25.11 ± 1.17 ***	15.88 ± 0.72 ns	24.53 ± 1.21	27.88 ± 1.43
pH 8	26.73 ± 1.33	31.85 ± 1.78 *	38.75 ± 1.97 ***	19.31 ± 0.91	23.62 ± 1.08 **	9.94 ± 0.64 ****	25.12 ± 1.34	29.41 ± 1.52
pH 9	23.85 ± 1.47	30.46 ± 1.55 ***	36.64 ± 1.84 ***	7.44 ± 0.41	21.34 ± 0.99 ****	3.01 ± 0.27 ****	23.46 ± 1.28	28.76 ± 1.46
pH 10	22.14 ± 1.22	29.10 ± 1.48 **	35.90 ± 1.79 ****	8.21 ± 0.45	18.92 ± 0.88 ****	2.73 ± 0.33 ****	22.38 ± 1.19	27.34 ± 1.37

D-fucose and potassium gluconate, and weak utilization of D- and L-arabinose, D- and L-xylose and 2- and 5-ketogluconate.

Fatty acid profiles (Supplementary Table S6) showed a strong predominance of Summed Feature 8 (primarily C18:1 ω7c/ω6c) across all strains analyzed, with particularly high relative abundances in strain 1A^T and *Mb. phyllostachyos* NBRC 105206^T. Other detected components included Summed Feature 3, Summed Feature 6, and Summed Feature 9, as well as minor amounts of straight-chain, hydroxylated, and branched-chain fatty acids (e.g., C14:1 ω5c, C16, C18, C17 iso/anteiso, and C20:2 ω6), with strain-dependent variation in their relative proportions. Strain 1A^T displayed a simplified profile dominated by Summed Feature 8, whereas strain 2A^T and *Mb. radiotolerans* JCM 2831^T showed a more diverse composition including multiple summed features and branched fatty acids. Overall, while the main fatty acid components were conserved among strains, differences in the relative abundance of minor constituents were observed. These patterns were consistent across at least three out of five biological replicates, in line with the known sensitivity of FAME profiles to culture conditions (Mező et al., 2022).

The predominant polar lipids detected by TLC in strain 1A^T, *Mb. radiotolerans* JCM 2831^T, strain 2A^T, and *Mb. guangdongense* KCTC 8298^T were phospholipids, including phosphatidylcholine, phosphatidylglycerol, and phosphatidylethanolamine (Supplementary Fig. S6).

These phenotypic and chemotaxonomic analyses indicated that strains 1A^T and 2A^T represent novel species, clearly differentiated from their closest phylogenetic relatives.

3.5. Differences in methylotrophic metabolism among closely related methylobacterium species

Strain 1A^T, *Mb. radiotolerans* JCM 2831^T, *Mb. oryzae* DSM 18207^T, strain 2A^T, and *Mb. guangdongense* KCTC 8298^T grew in MM supplemented with methanol in the presence or absence of $LaCl_3$ (Ln) (Fig. 2A and Supplementary Fig. S7A). Strain 2A^T and *Mb. guangdongense* KCTC 8298^T reached higher OD_{600} values at the end of the incubation period and showed significantly higher AUC values than all other strains under these conditions ($p < 0.0001$; Supplementary Fig. S7A). Strain 1A^T also showed significantly higher AUC than *Mb. phyllostachyos* NBRC 105206^T, *Mb. longum* DSM 23933^T, and *Mb. tardum* NBRC 103632^T in the absence of Ln (Supplementary Fig. S7A). In contrast, *Mb. phyllostachyos* NBRC 105206^T, *Mb. longum* DSM 23933^T, and *Mb. tardum* NBRC 103632^T exhibited minimal increases in OD_{600} throughout the incubation period in MM methanol, either in the presence or absence of Ln, reflected in their AUC. The presence of Ln did not significantly affect AUC within any strain, although OD_{600} at 60 h was slightly higher with Ln in *Mb. phyllostachyos*, *Mb. longum* and *Mb. tardum* (Fig. 2A).

Strain 2A^T and *Mb. guangdongense* KCTC 8298^T showed robust growth in MM ethanol, whereas strain 1A^T and *Mb. radiotolerans* JCM 2831^T displayed moderate and limited growth, respectively. The addition of Ln slightly enhanced the growth of strain 1A^T and *Mb. guangdongense* KCTC 8298^T (Fig. 2B). *Mb. tardum* NBRC 103632^T did not show detectable growth, whereas the remaining strains exhibited very limited growth under these conditions (Table 1, Supplementary Fig. S7B). Overall, these results indicate metabolic differences among these closely related species.

3.6. Comparison of PGP traits of the related methylobacterium species

3.6.1. Utilization of ACC

The ability of the eight strains to utilize ACC *in vitro* was evaluated using DF minimal medium supplemented with ACC as the sole nitrogen source. Although all strains harbor the ACC deaminase gene, growth under this condition varied substantially among strains. Strain 2A^T showed the highest OD_{600} values and AUC, while increases in OD_{600} were also observed in *Mb. radiotolerans* JCM 2831^T and *Mb. guangdongense* KCTC 8298^T. Lower increases in OD_{600} were observed for *Mb. tardum* NBRC 103632^T, *Mb. phyllostachyos* NBRC 105206^T, and strain 1A^T, whereas *Mb. longum* DSM 23933^T and *Mb. oryzae* DSM 18207^T showed no detectable growth under these conditions (Fig. 3). AUC values in DF + ACC were significantly higher than in DF alone for *Mb. radiotolerans* JCM 2831^T, strain 2A^T, *Mb. guangdongense* KCTC 8298^T, *Mb. phyllostachyos* NBRC 105206^T, and *Mb. tardum* NBRC 103632^T ($p < 0.0001$), whereas no significant difference between conditions was observed for strain 1A^T, *Mb. oryzae*, or *Mb. longum* (Supplementary Fig. S8). Since growth in DF-ACC medium provides an indirect indication of ACC deaminase functionality, these results suggest differential capacities among strains to utilize ACC-derived nitrogen rather than providing a direct quantitative measurement of ACC deaminase enzymatic activity.

3.6.2. Production of phytohormones

In vitro, all strains produced detectable amounts of IAA in the presence of Trp, with mean concentrations ranging from 2.23 ± 0.28 to 9.45 ± 1.31 μg per 5 mL of inoculated culture, corresponding to 0.45 ± 0.06 to 1.89 ± 0.26 μg/mL (Fig. 4A). *Mb. oryzae* DSM 18207^T showed the highest IAA production, while strain 2A^T showed the lowest, differing significantly from all other strains ($p \leq 0.044$) except *Mb. brachiatum* NBRC 103629^T (3.73 ± 2.97 μg per 5 mL; 0.75 ± 0.59 μg/mL). In contrast to IAA, which was produced at μg levels, SA and CKs were detected at ng-level concentrations, with significantly higher SA production observed in strain 2A^T (21.52 ± 1.61 ng per 5 mL; 4.30 ± 0.32 ng/mL) and *Mb. guangdongense* KCTC 8298^T (20.35 ± 3.20 ng per 5 mL; 4.07 ± 0.64 ng/mL) compared with the other tested strains ($p < 0.0001$; no significant difference between these two strains) (Fig. 4B). Mean iP concentrations ranged from 0 to 0.55 ± 0.30 ng per 5 mL culture (0 to 0.11 ± 0.06 ng/mL) and were not significantly different among strains, except that *Mb. oryzae* DSM 18207^T differed significantly from *Mb. radiotolerans* JCM 2831^T ($p = 0.0061$), strain 2A^T ($p = 0.0061$), and *Mb. brachiatum* NBRC 103629^T ($p = 0.0197$) (Fig. 4C). Mean tZ concentrations ranged from 0.07 ± 0.13 to 1.87 ± 0.10 ng per 5 mL culture (0.014 ± 0.026 to 0.37 ± 0.02 ng/mL). *Mb. brachiatum* NBRC 103629^T showed significantly higher tZ levels than all strains except *Mb. longum* DSM 23933^T ($p \leq 0.039$), while *Mb. longum* DSM 23933^T also differed significantly from strain 1A^T, *Mb. oryzae* DSM 18207^T, strain 2A^T, *Mb. phyllostachyos* NBRC 105206^T, and *Mb. tardum* NBRC 103632^T ($p \leq 0.039$) (Fig. 4D). Other phytohormones, including ABA, JA, JA-Ile, and GAs, were not detected under the conditions tested.

Because bacterial growth differed among strains under the assay conditions, ranging from approximately 4×10^6 CFU/mL in *Mb. tardum* NBRC 103632^T to 8×10^7 CFU/mL in *Mb. oryzae* DSM 18207^T, IAA and SA production were additionally expressed as ng per 10^6 CFU. Although total IAA production was highest in *Mb. oryzae* DSM 18207^T, normalization by CFU revealed that *Mb. tardum* NBRC 103632^T (358.86 ± 7.28 ng per 10^6 CFU) and *Mb. phyllostachyos* NBRC 105206^T (165.09 ± 13.30 ng per 10^6 CFU) showed significantly higher IAA production on a per-cell basis than all other strains ($p < 0.0001$; Supplementary Fig. S9, **left panel**), while strain 2A^T showed the lowest values overall, differing significantly from most strains except *Mb. oryzae* DSM 18207^T and *Mb. brachiatum* NBRC 103629^T. In contrast, normalization did not alter which strains produced the most SA, with strain 2A^T and *Mb. guangdongense* KCTC 8298^T remaining the highest producers on both a total and per-cell basis (Supplementary Fig. S9, **right panel**). Therefore, total hormone production per culture was retained for comparisons among strains because it reflects the overall hormone output achieved under the tested conditions.

3.6.3. Methylobacterium species differentially promote plant growth

Given their shared PGP-related genes and their ability to produce IAA and CKs, we evaluated whether the remaining *Methylobacterium* strains exhibited PGP effects similar to those previously reported for strain 2A^T (Grossi et al., 2020, 2024). At 3 dpi, no strain significantly altered LR density relative to the uninoculated control (Fig. 5A). By 5

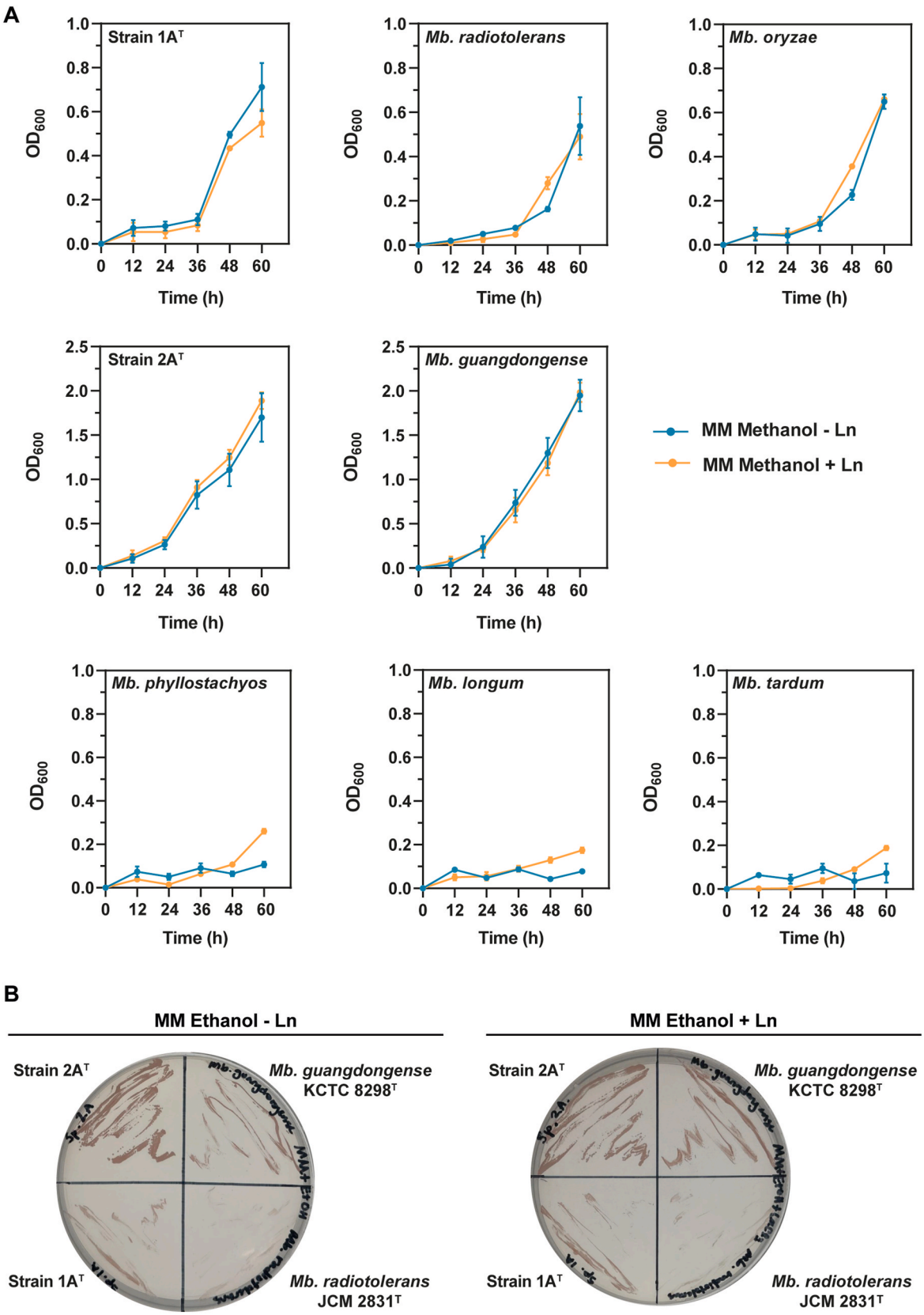

Fig. 2. Growth of *Methylobacterium* strains in minimal medium containing methanol or ethanol, with or without Ln. (A) Growth curves of eight *Methylobacterium* strains cultured in minimal medium with methanol (MM Methanol) or minimal medium with methanol supplemented with 30 μM $LaCl_3$ (MM Methanol + Ln). Growth was monitored by measuring OD_{600} every 12 h for 60 h. Each panel represents a different strain. Data points represent the mean ± SD of three measurements. OD_{600} values are blank-corrected and converted to a 1-cm path length. **(B)** Representative images of colonies grown on MM plates containing ethanol (0.5%) with or without Ln.

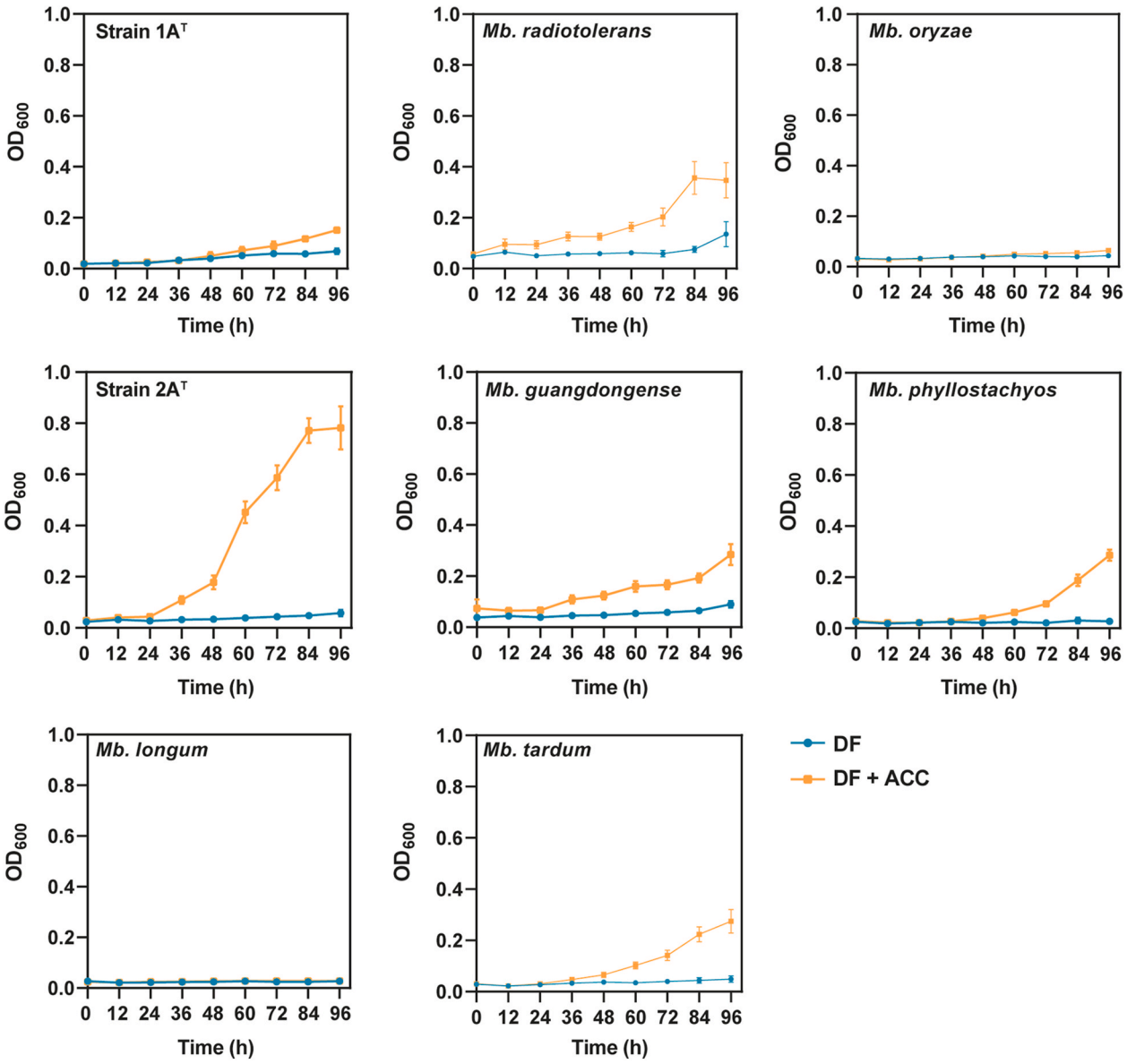

Fig. 3. Growth of *Methylobacterium* strains in DF minimal medium with and without ACC as nitrogen source. Growth was assessed in DF minimal salts medium in the absence (DF) or presence (DF + ACC) of ACC as the sole nitrogen source. Growth was monitored by measuring OD_{600} every 12 h for 96 h. Each panel represents a different strain. Data points represent the mean ± SD of three measurements.

dpi, strain 1A^T significantly increased LR density in *A. thaliana* compared with the uninoculated control (0.19 ± 0.01 versus 0.11 ± 0.01 LR/mm PR; $p = 0.0111$), and also produced significantly higher LR density than *Mb. radiotolerans* JCM 2831^T, *Mb. longum* DSM 23933^T, and *Mb. tardum* NBRC 103632^T ($p = 0.03$, $p = 0.004$ and $p = 0.0001$, respectively). Although *Mb. oryzae* DSM 18207^T (0.15 ± 0.02 LR/mm PR) and *Mb. tardum* (0.06 ± 0.02 LR/mm PR) showed numerically higher and lower LR density than the control at 5 dpi, respectively, neither difference reached statistical significance (Fig. 5A).

Inoculation experiments with wheat and barley seeds revealed plant species-dependent effects on seedling development. In wheat, inoculation with strain 1A^T ($p < 0.0001$), *Mb. oryzae* DSM 18207^T ($p = 0.0334$), and *Mb. longum* DSM 23933^T ($p < 0.0001$) significantly increased hypocotyl length compared with the uninoculated control, reaching 1.38 ± 0.04, 1.19 ± 0.05, and 1.37 ± 0.05 (relative to the control), respectively, compared with 1.00 ± 0.03 in the control (Fig. 5B, left panel). These findings are consistent with previous observations for strain 2A^T (Grossi et al., 2024). A slight but significant effect ($p = 0.0438$) on root number was observed in roots inoculated with *Mb. radiotolerans* JCM 2831^T (Fig. 5B, right panel).

In barley, only *Mb. radiotolerans* JCM 2831^T significantly increased hypocotyl length ($p < 0.0001$), reaching 2.47 ± 0.13 compared with 1.00 ± 0.08 in the control. Inoculation with strain 1A^T, *Mb. oryzae*, and *Mb. tardum* also resulted in a slight increase in hypocotyl length, with mean values of 1.39 ± 0.12, 1.39 ± 0.12, and 1.38 ± 0.15, respectively, although these effects were not statistically significant (Fig. 5C, left panel). In addition, inoculation with *Mb. phyllostachyos* NBRC 105206^T significantly increased root number compared with the control ($p < 0.0001$), with mean values of 1.33 ± 0.02 versus 1.00 ± 0.01 in the control (Fig. 5C, right panel).

3.6.4. Biofilm forming capacity

Pink pigmentation was visibly evident on the primary roots of *A. thaliana* seedlings inoculated with strain 1A^T, strain 2A^T, *Mb. phyllostachyos* NBRC 105206^T, *Mb. oryzae* DSM 18207^T, and *Mb. radiotolerans* JCM 2831^T. In contrast, no such pigmentation was observed in

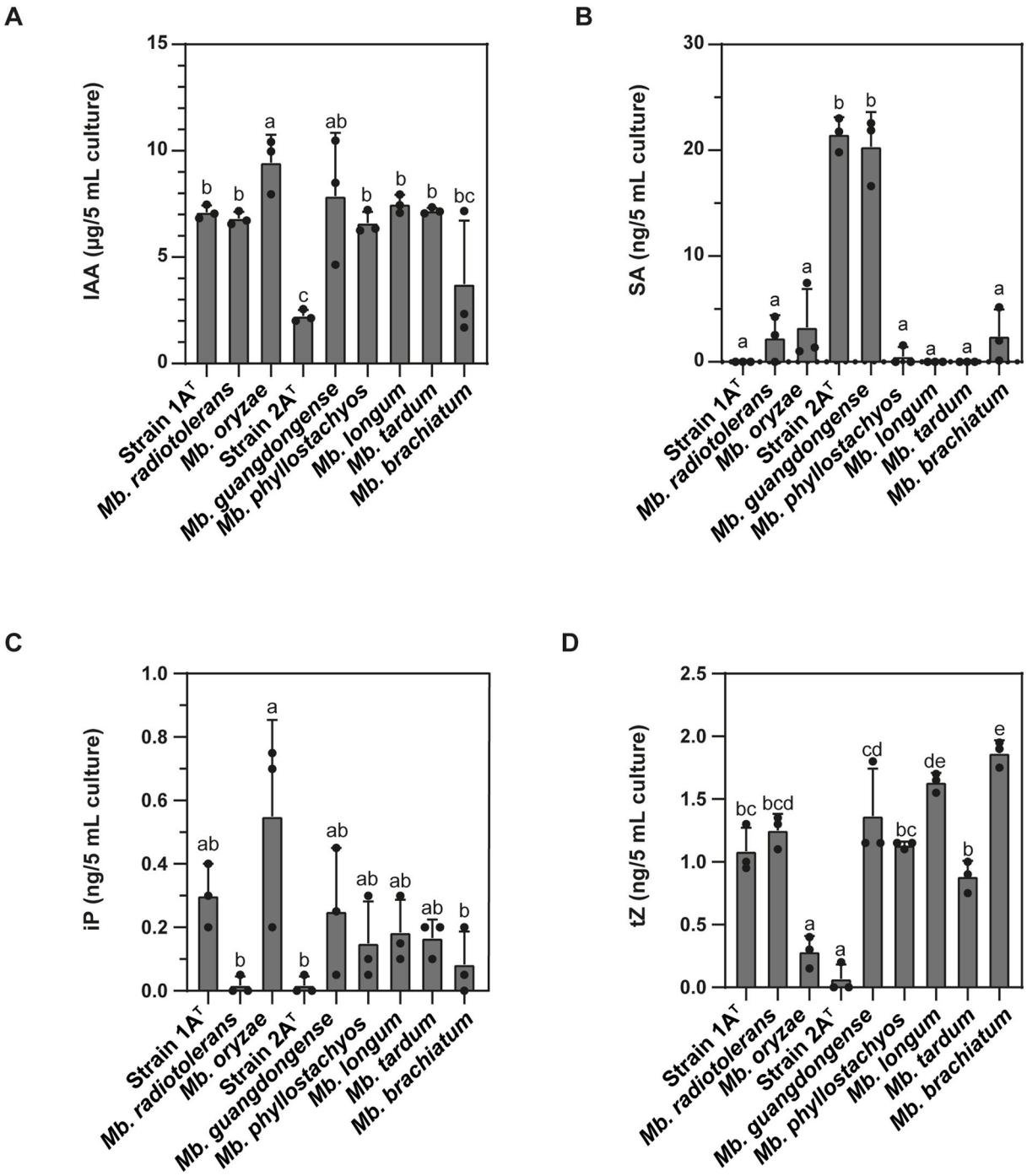

Fig. 4. Phytohormone production by *Methylobacterium* species after 5 days of growth in R2A medium supplemented with 1 g/L tryptophan. (A) Indole-3-acetic acid (IAA), **(B)** salicylic acid (SA), **(C)** isopentenyladenine (iP), and **(D)** trans-zeatin (tZ). Hormone levels were expressed as µg/5 mL of inoculated culture for IAA and as ng/5 mL of inoculated culture for SA, iP, and tZ and calculated as the difference between inoculated cultures and uninoculated control medium. Concentrations in the culture supernatant (µg/mL for IAA; ng/mL for SA, iP, and tZ) are given in the text. Individual data points represent three biological replicates, and bars represent mean ± SD. Statistical significance was determined by one-way ANOVA followed by Tukey's HSD test. Different letters indicate significant differences ($p < 0.05$).

plants inoculated with *Mb. longum* DSM 23933^T or *Mb. tardum* NBRC 103632^T (Fig. 6A, upper panel). However, upon closer examination using the stereomicroscope, a faint pink matrix was observed surrounding the primary roots (Fig. 6A, lower panel). These visual observations suggest an association of the inoculated strains with the root surface and may reflect the establishment of surface-associated communities, potentially including biofilm formation.

We then evaluated the biofilm-forming capacity of these type strains on an inert surface. Among them, strain 2A^T exhibited a crystal violet staining pattern comparable to that of the PGPR *Azospirillum brasilense* Az39, used as a positive control due to its well-documented biofilm-forming capacity (Díaz Herrera et al., 2016). This qualitative assay indicated that strain 2A^T, *Mb. longum*, and *Mb. tardum*, and to a lesser extent strain 1A^T, showed detectable biofilm-associated adhesion in the crystal violet assay (Fig. 6B).

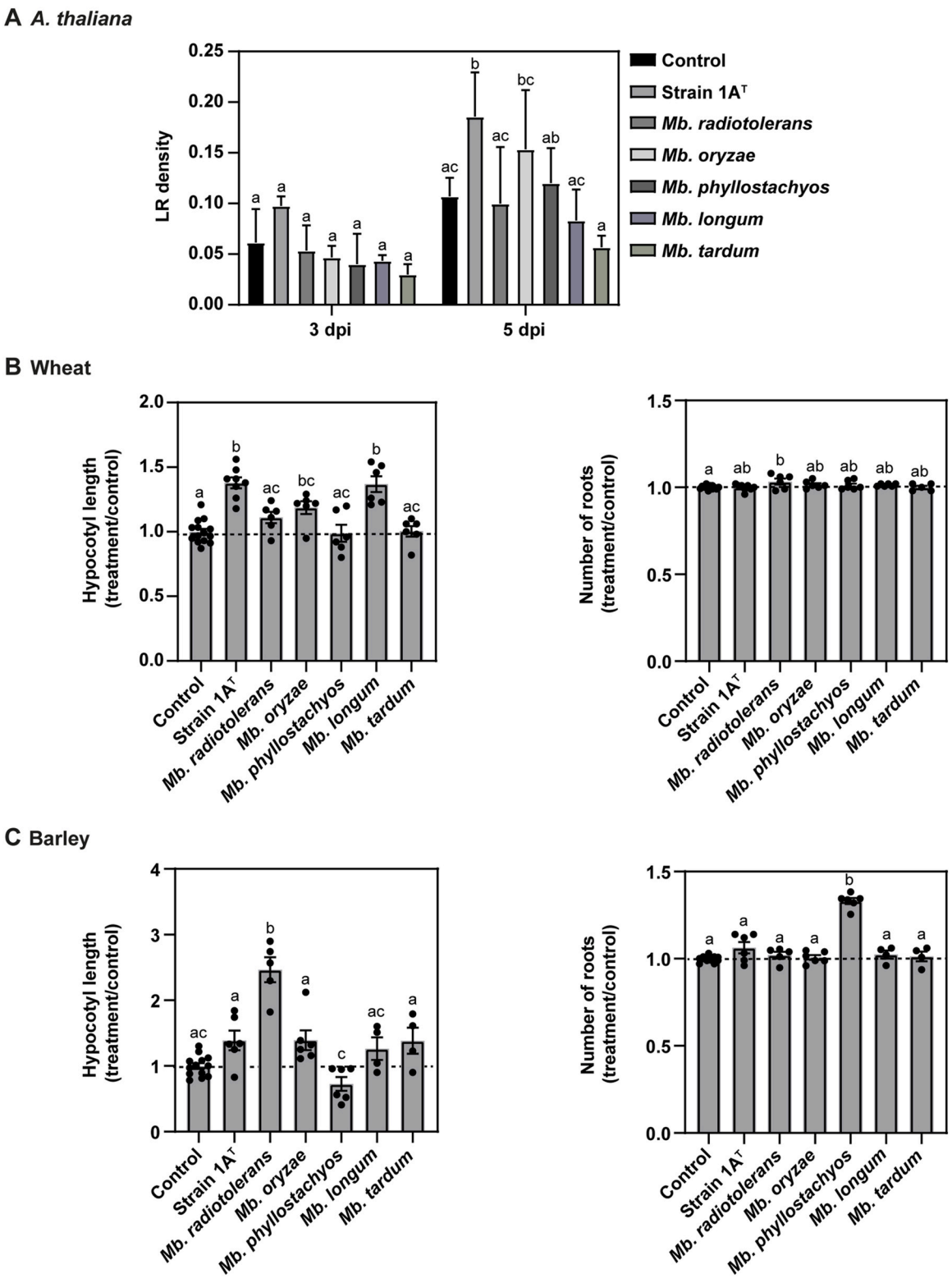

Fig. 5. Differential effects of *Methylobacterium* strains on *A. thaliana* plantlets (A) and on wheat (B) and barley (C) seedlings. Inoculation was performed with strain 1A^T, *Mb. phyllostachyos* NBRC 105206^T, *Mb. radiotolerans* JCM 2831^T, *Mb. oryzae* DSM 18207^T, *Mb. longum* DSM 23933^T, or *Mb. tardum* NBRC 103632^T. Lateral root density (LR/mm PR) was measured in *A. thaliana* **(A)**, while hypocotyl length (cm) and root number were measured in wheat **(B)** and barley **(C)** seedlings and expressed relative to the non-inoculated control. **(A)** LR density in *A. thaliana* seedlings at 3 and 5 dpi following inoculation with selected *Methylobacterium* species. Data represent means ± SD, where each point corresponds to one biological replicate consisting of five plants. Statistical significance was determined by two-way ANOVA followed by Tukey's HSD test ($p < 0.05$). Different letters above the bars indicate significant differences among treatments and time points. **(B-C)** Bars represent means ± SEM of independent biological replicates. Each dot represents one independently inoculated plate containing 25 seedlings. Values were calculated as the ratio between the mean value of the 25 seedlings in each inoculated plate and the mean value of the non-inoculated control plates from the same experimental run. A larger number of non-inoculated control replicates was included to obtain a robust estimate of the baseline values for the measured parameters. Statistical significance was determined by one-way ANOVA followed by Tukey's HSD multiple-comparisons test ($p < 0.05$).

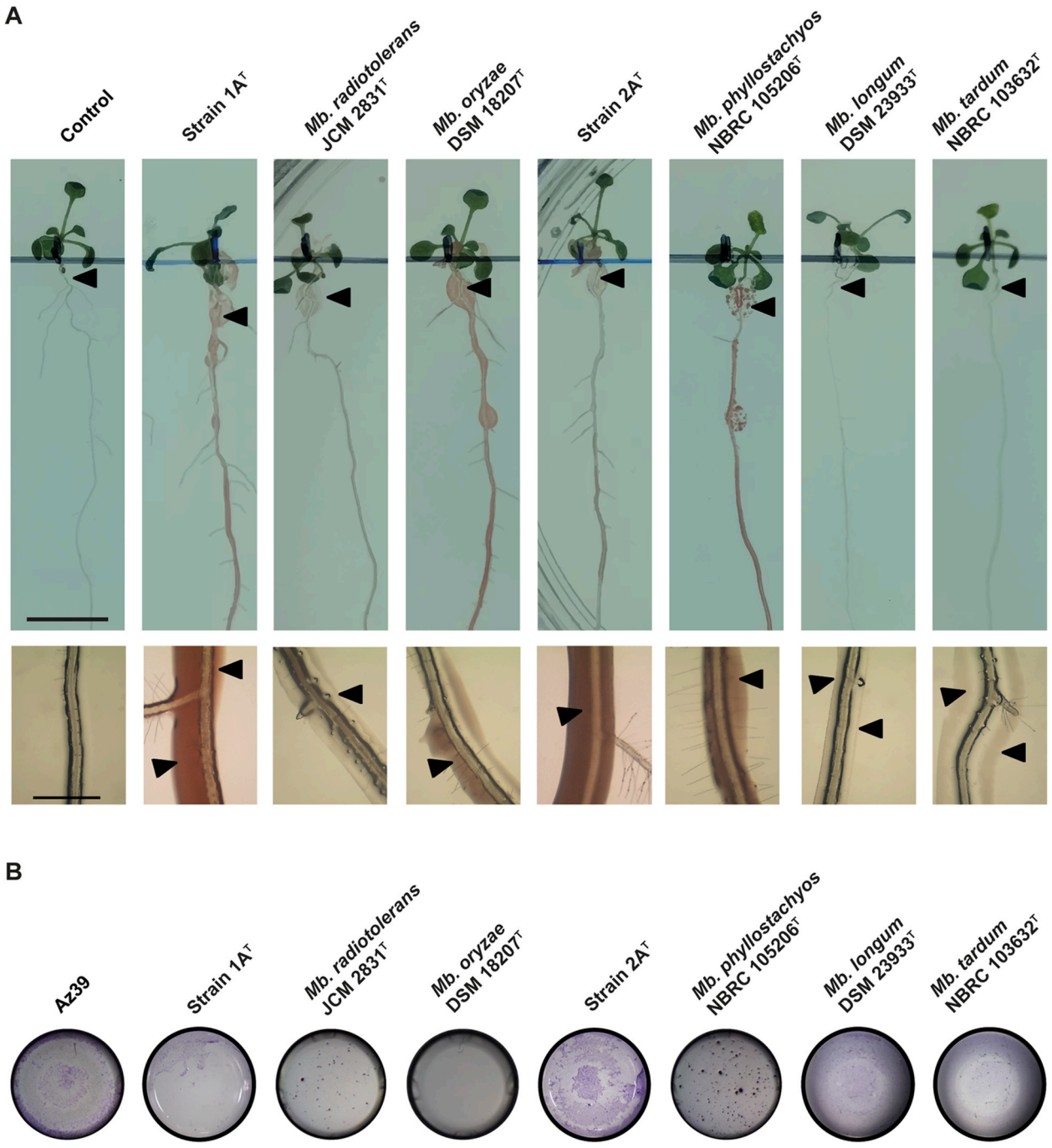

Fig. 6. Association with *A. thaliana* roots and biofilm formation in *Methylobacterium* species. (A) Upper panel: Representative images of 10-day-old *A. thaliana* plants inoculated with strain 1A^T, *Mb. radiotolerans* JCM 2831^T, *Mb. oryzae* DSM 18207^T, strain 2A^T, *Mb. phyllostachyos* NBRC 105206^T, *Mb. longum* DSM 23933^T, *Mb. tardum* NBRC 103632^T or mock-inoculated (control). Black triangles denote the inoculation site. Bar: 1 cm. Lower panel: Close-up images acquired using a Leica stereomicroscope at 5 dpi, with black triangles indicating areas of pink pigmentation. Bar: 0.5 cm. **(B)** Crystal violet staining of cells attached to the bottom of 96-well microtiter plates for each bacterial species. One representative well per strain (n = 4) is shown. *Azospirillum brasilense* Az39 was included as a positive control.

3.6.5. *Production of N-acyl-homoserine lactones*

Quorum sensing (QS) genes regulate biofilm development by sensing population density through signaling molecules such as AHLs (Swift et al., 2001). The *Methylobacterium* strains were tested for their ability to produce AHL signaling molecules using different biosensors. Strain 1A^T, strain 2A^T, and *Mb. radiotolerans* JCM 2831^T induced violacein production in both *C. violaceum* biosensor strains. Among them, strain 2A^T showed stronger violacein induction in VIR07 compared with the other tested strains, indicating the production of C10 AHLs. In contrast, *Mb. longum* DSM 23933^T and *Mb. guangdongense* KCTC 8298^T elicited weak violacein production exclusively in strain VIR07. Conversely, *Mb. phyllostachyos* NBRC 105206^T, *Mb. oryzae* DSM 18207^T, and *Mb. tardum* NBRC 103632^T did not induce violacein production in any of the biosensor strains (Supplementary Table S7A).

4. Discussion

The physiological and metabolic heterogeneity observed among closely related *Methylobacterium* species (Tables 1 and 2; Supplementary Tables S4 and S5) suggests niche-specific adaptations that may influence

their ecological fitness and interactions with plants. *Mr. extorquens* AM1 produces a diverse array of enzymes that enable the utilization of substrates such as methanol and ethanol in nutrient-poor environments like the phyllosphere, providing a significant metabolic advantage (Sy et al., 2005). Strain 2A^T and *Mb. guangdongense* showed higher OD_{600} and AUC values on methanol, while others such as *Mb. phyllostachyos, Mb. longum*, and *Mb. tardum* exhibited limited or delayed growth (Fig. 2A; Supplementary Fig. S7A), highlighting metabolic diversification within the group. While most of the tested strains harbor a complete *mxa* cluster, this was absent in *Mb. longum* and *Mb. tardum* (Supplementary Table S3) and could explain their inability to grow on methanol in the absence of Ln. Given that XoxF is activated in the presence of Ln (Tani et al., 2021), the presence of the *xoxF* gene may account for the slight growth of *Mb. phyllostachyos*, *Mb. longum,* and *Mb. tardum* on methanol when Ln is available (Fig. 2A). All strains encode an ExaF enzyme; however, only strain 2A^T, strain 1A^T, and *Mb. guangdongense* efficiently used ethanol as the sole carbon source (Fig. 2B; Supplementary Fig. S7B). This difference may be due to variations in ExaF kinetic properties, as previously reported for similar XoxF5 and ExaF enzymes (Huang et al., 2019; Good et al., 2016).

Although all strains encode ACC deaminase-related genes, only strain 2A^T, *Mb. guangdongense*, *Mb. radiotolerans, Mb. phyllostachyos* and *Mb. tardum* displayed substantial growth in DF medium supplemented with ACC as the sole nitrogen source **(**Supplementary Fig. S8**)**. This result indicates that gene presence alone is not necessarily associated with efficient ACC utilization. Because growth in DF-ACC medium provides only an indirect estimate of ACC deaminase activity, additional biochemical assays would be required to quantify enzymatic activity and confirm functional differences among strains. Nevertheless, the observed growth patterns suggest that these strains may possess a greater capacity to metabolize ACC and potentially modulate plant ethylene levels through ACC degradation, thereby contributing to the alleviation of stress-related ethylene responses (Grossi et al., 2025).

The ability of the strains to produce phytohormones *in vitro* revealed clear functional differences among them. All strains harbor the IAN pathway and produce IAA under the tested conditions (Fig. 4A). However, strain 2A^T and *Mb. brachiatum*, which also harbor the *iaaM* gene, showed lower IAA production (Fig. 4A; Supplementary Fig. S9), indicating that the presence of this additional biosynthetic gene alone is insufficient to predict auxin output and suggesting the involvement of regulatory or metabolic constraints. Consistent with previous reports (Palberg et al., 2022), tZ was the predominant cytokinin detected among the analyzed strains, whereas iP levels remained low, except in *Mb. oryzae* DSM 18207^T. Notably, CK levels in strain 2A^T were negligible (Fig. 4C and D). Moreover, strain 2A^T and *Mb. guangdongense* produced SA (Fig. 4B) as has been reported for other PGPRs (Bakker et al., 2014). Bakker et al. suggest that in natural environments SA is more likely incorporated into SA-derived metabolites, particularly siderophores, rather than released in its free form. In the case of strain 2A^T, its combination with negligible CK production further defines a distinct hormonal profile that may underlie a specific functional strategy in plant-microbe interactions.

Microbially produced IAA plays a pivotal role in plant-microbe interactions, acting as a signaling molecule that influences plant growth, development, and physiological responses (Spaepen and Vanderleyden, 2010). Strain 2A^T can modulate *A. thaliana* root architecture through IAA biosynthesis (Grossi et al., 2024), and other studies reported that *Mb. oryzae*, *Mb. radiotolerans*, and *Mb. tardum* improved crop growth (Madhaiyan et al., 2009; Chanratana et al., 2017; Priya et al., 2019). In the present study, strain 1A^T significantly increased LR density in *A. thaliana*, whereas *Mb. tardum* showed a non-significant trend toward lower LR density (Fig. 5A). In line with these observations, assays in wheat and barley further revealed strain- and plant species-dependent effects on seedling development, with growth promotion varying across bacterial strains and plant species (Fig. 5B–C), highlighting that PGP outcomes are context-dependent and not solely predicted by genomic potential or *in vitro* hormone production.

Biofilm formation is a key trait of PGPR, as it enhances root colonization and persistence in competitive soil environments, largely through QS-regulated mechanisms (Begum et al., 2019; Velmourougane et al., 2017). Our results indicated that strain 2A^T, *Mb. longum*, and *Mb. tardum*, and to a lesser extent strain 1A^T, were capable of biofilm formation. This is in agreement with Park et al. (2020), who identified *Mb. longum* and *Mb. tardum* as high biofilm formers and *Mb. radiotolerans* as a normal biofilm former. In Gram-negative bacteria, QS signaling is mediated by AHLs, which promote cell aggregation and facilitate effective plant colonization (Begum et al., 2019). Only strain 1A^T, strain 2A^T, and *Mb. radiotolerans* JCM 2831^T produced both short- and long-chain AHL molecules (Supplementary Table S7A), suggesting an enhanced capacity for cell-cell communication. AHL signals are typically synthesized by LuxI-type acyl-HSL synthases, while LuxR-family regulators mediate QS-dependent gene expression (Parsek and Greenberg, 2000).

The genomes of strains 1A^T and 2A^T contained 16 and six putative *luxR* homologs, respectively. BLAST searches using LuxR (MpoR; MPOP_5029) and LuxI (MpoI; MPOP_5028) from *Mr. populi* as queries were conducted against the genomes of the eight Group A strains. Most of the analyzed species harbor a canonical LuxI/LuxR system, typically consisting of a LuxR-family regulator located upstream of a predicted AHL synthase gene, although sequence identity varies among species. LuxI/LuxR proteins from strain 1A^T showed high sequence identity with those of *Mb. radiotolerans* JCM 2831^T and *Mb. oryzae* DSM 18207^T. In contrast, strain 2A^T and *Mb. phyllostachyos* NBRC 105206^T shared similar LuxR homologs, although no LuxI homolog was detected in *Mb. phyllostachyos* NBRC 105206^T. Notably, *Mb. guangdongense* KCTC 8298^T displayed higher LuxI/LuxR similarity to *Mb. longum* DSM 23933^T than to strain 2A^T. No LuxI/LuxR homologs were identified in *Mb. tardum* NBRC 103632^T (Supplementary Table S7B).

The visible pink pigmentation observed on *A. thaliana* roots, together with AHL production and biofilm formation, suggests that these *Methylobacterium* isolates possess traits that may contribute to surface-associated interactions with plants. Since successful root colonization is influenced by multiple microbial traits, including adhesion, biofilm formation, survival, and intercellular communication (Beauregard et al., 2013; Meneses et al., 2011; Danhorn and Fuqua, 2007), these characteristics may contribute to the ability of these strains to interact with plant surfaces. However, further studies will be required to determine the specific contribution of quorum sensing in root colonization and plant-associated fitness.

Genomic analysis identified mercury and arsenate resistance genes in strains 1A^T and 2A^T, many associated with mobile genetic elements (Supplementary Fig. S3), highlighting the role of HGT in shaping lineage-specific adaptive traits and suggesting potential for environmental resilience and bioremediation. Consistently, Samanta et al. (2024) reported frequent HGT in shell and cloud regions among type II methylotrophs, underscoring the importance of accessory genomes in environmental adaptation.

Based on genomic and phylogenetic analyses, strains 1A^T and 2A^T are assigned to the genus *Methylobacterium* within Group A. Both can be proposed as candidate novel species within the genus based on ANI and dDDH values. These results distinguish strain 2A^T from *Mb. guangdongense* and *Mb. phyllostachyos*, and strain 1A^T from *Mb. radiotolerans* and *Mb. oryzae*. The concordance between phylogenomic topology and genome similarity metrics strongly supports their recognition as two distinct novel species. Moreover, their taxonomic position in Group A (Fig. 1) is consistent with the framework proposed by Leducq et al. (2022), who assigned strain 2A^T to subclade A9 based on a clade-specific *rpoB* marker.

In addition to the genomic evidence, the novel strains exhibited distinct physiological characteristics under identical experimental conditions, further supporting their differentiation from their closest relatives and being consistent with the ANI and dDDH relatedness patterns described above. Temperature tolerance in R2A distinguished the two

novel strains, as strain 1A^T did not grow at 37 °C, whereas strain 2A^T grew under this condition. Furthermore, strain 1A^T differed from *Mb. radiotolerans* and *Mb. oryzae*, both of which grew at all temperatures tested (24, 30, and 37 °C), while strain 2A^T differed from *Mb. guangdongense* and *Mb. phyllostachyos*, neither of which grew at 37 °C (Table 1). Likewise, both strains tolerated NaCl concentrations up to 0.5% (w/v) but failed to grow at 1% NaCl in either R2A or LBNS medium. This profile distinguished strain 1A^T from *Mb. radiotolerans* and *Mb. oryzae*, which tolerated 1% NaCl in both media, and strain 2A^T from *Mb. guangdongense* and *Mb. phyllostachyos*, which retained growth at 1% NaCl in R2A medium (Table 1). Evaluation of growth across pH 5-10 further highlighted physiological differences among the strains. While strain 1A^T maintained growth throughout the entire pH range tested, strain 2A^T exhibited lower growth rates under alkaline conditions (pH 9-10), as reflected by lower μ_{app} and AUC values (Table 2; Supplementary Fig. S5). In contrast, *Mb. guangdongense* exhibited a less pronounced decline under the same conditions. These growth parameters are turbidity-based and were obtained under a uniform measurement procedure; while per-cell optical properties may differ among strains, the magnitude of the differences reported here exceeds what such variation would be expected to produce. Together with the biochemical and chemotaxonomic characteristics, these physiological traits complement the phylogenomic evidence and support the recognition of strains 1A^T and 2A^T as two novel species within the genus *Methylobacterium*, for which the names *Methylobacterium solani* sp. nov. and *Methylobacterium torresii* sp. nov. are proposed.

5. Description of the novel species

5.1. Description of *Methylobacterium solani* sp. nov

Methylobacterium solani (so.la'ni. L. gen. neut. n. *solani*, of Solanum)

Cells are Gram-stain-negative, aerobic, pink-pigmented, rod-shaped and motile. Colonies are small, circular, smooth, ~0.06 mm diameter after 3 days at 28 °C on R2A agar. Grows well on PDA and RSA media. Catalase, oxidase, urease and glucose fermentation are positive. Nitrate reduction negative. The following compounds are utilized as sole carbon and energy sources: D-glucose (weak), gluconate, adipic acid (weak), malic acid (weak), glycerol, D-arabinose (weak), D-lyxose (weak). Utilizes methanol and ethanol as sole carbon sources both in the presence and absence of lanthanides. The phenotypic and chemotaxonomic characteristics are detailed in the main text and in Table 1. The predominant phospholipids as detected by TLC are phosphatidylcholine, phosphatidylglycerol, and phosphatidylethanolamine. The major fatty acid is Summed Feature 8 (comprised 18:1 ω7c/18:1 ω6c) and C14.1ω5c. The draft genome of the type strain is 7.13 Mb, and its genomic DNA G + C content is 70.9%.

The type strain, 1A^T (= RGM 3871^T = DSM 121859^T), was isolated in November 2021 from the roots of potato (*Solanum tuberosum* L. cv. Désirée) plants at INGEBI-CONICET (Argentina). The GenBank/EMBL/DDBJ accession number of the 16S rRNA gene is PX853811, whereas that of the draft genome sequence of strain 1A^T is JBYQVE000000000.

5.2. Description of *Methylobacterium torresii* sp. nov

Methylobacterium torresii (tor.re.si'i. N.L. gen. masc. n. *torresii*, of Torres, in honour of Dr. Héctor N. Torres, a renowned scientist whose greatest legacy was the foundation of INGEBI-CONICET).

Cells are Gram-stain-negative, aerobic, pink-pigmented, rod-shaped, and motile. Colonies on R2A agar are small, circular, firm, dry, hard, and brittle, measuring ~0.2 mm diameter after 3 days at 28 °C. Growth also occurs at 37 °C. Grows well on PDA and RSA media. Catalase, oxidase, urease and arginine dihydrolase are positive. Nitrate reduction negative. Utilizes methanol and ethanol as sole carbon sources both in the presence and absence of lanthanides. The following compounds are utilized as sole carbon and energy sources: L-arabinose, D-mannose (weak), gluconate, adipic acid (weak), glycerol, D-arabinose (weak), D-xylose (weak), L-xylose (weak), D-fructose, D-lyxose, D-fucose, 2-ketogluconate (weak), 5-ketogluconate (weak). The phenotypic and chemotaxonomic characteristics are detailed in the main text and in Table 1. The predominant phospholipids as detected by TLC are phosphatidylcholine, phosphatidylglycerol, and phosphatidylethanolamine. The major fatty acids are Summed Feature 8 (comprised 18:1 ω7c/18:1 ω6c), Summed Feature 9 (17:1 iso ω9c/16:0 10-methyl), C15.0 anteiso, and C12.0 2-OH. The draft genome of the type strain is 6.40 Mb, and its genomic DNA G + C content is 69.5%.

The type strain, 2A^T (= RGM 3872^T = DSM 121860^T), was isolated in January 2017 from the roots of potato (*Solanum tuberosum* L. cv. Désirée) at INGEBI-CONICET (Argentina). The GenBank/EMBL/DDBJ accession numbers of the 16S rRNA gene and draft genome sequence of strain 2A^T are MG818293.2 and VUOK00000000, respectively.

CRediT authorship contribution statement

Cecilia Eugenia María Grossi: Conceptualization, Investigation, Methodology, Validation, Visualization, Writing – original draft. **Allison Renee Megow:** Methodology, Investigation, Validation, Writing – review and editing. **Edgar Martínez-Moyano:** Methodology, Validation, Writing – review and editing. **Md. Asif Mahamud:** Methodology, Investigation, Validation, Writing – review and editing. **Julieta Mariana Covelli:** Methodology, Validation, Writing – review and editing. **Takakazu Matsuura:** Methodology, Validation, Writing – review and editing. **Akio Tani:** Conceptualization, Investigation, Methodology, Project administration, Funding acquisition, Supervision, Validation, Visualization, Writing – review and editing. **Nurettin Sahin:** Conceptualization, Investigation, Methodology, Validation, Visualization, Writing – review and editing. **Rita María Ulloa:** Conceptualization, Investigation, Methodology, Project administration, Funding acquisition, Supervision, Validation, Visualization, Writing – original draft.

Declaration of competing interest

The authors declare that they have no known competing financial interests or personal relationships that could have appeared to influence the work reported in this paper.

Acknowledgments

This work was funded by Proyecto BID PICT 2021 #0440 and supported by the Joint Usage/Research Center, Institute of Plant Science and Resources, Okayama University, Ohara Foundation, and the JSPS Program for Forming Japan's Peak Research Universities (J-PEAKS, Grant Number JPJS00420230010). We want to thank Dr. Tomohiro Morohoshi (Utsunomiya Univ., Japan) and Dr. Paul Williams (Univ. Nottingham, UK) who kindly provided the *Chromobacterium violaceum* strains used in this project. Cecilia E. M. Grossi is a postdoctoral fellow from Agencia Nacional de Promoción de la Investigación, el Desarrollo Tecnológico y la Innovación. Rita M. Ulloa is a member of Carrera de Investigador Científico from CONICET and Associate Professor at Universidad de Buenos Aires (UBA).

Appendix A. Supplementary data

Supplementary data to this article can be found online at https://doi.org/10.1016/j.plaphy.2026.111988.

Data availability

The genome sequence of *Methylobacterium* sp. 1A (strain 1A^T) generated in this study is available in GenBank under accession JBYQVE000000000 (BioProject PRJNA1402344; BioSample SAMN54592014; RefSeq assembly GCF_058072805.1). The genome

sequence of *Methylobacterium* sp. 2A (strain 2A^T) was generated in a previous study (Grossi et al., 2020) and is available under accession VUOK00000000 (BioProject PRJNA560067; BioSample SAMN12567564; RefSeq assembly GCF_009806555.1); it was not re-sequenced here. The 16S rRNA gene sequences of strains 1A^T and 2A^T are available under accessions PX853811 and MG818293.2, respectively.

References

Alamgir, K.M., Masuda, S., Fujitani, Y., Fukuda, F., Tani, A., 2015. Production of ergothioneine by *Methylobacterium* species. Front. Microbiol. 6, 1185. https://doi.org/10.3389/fmicb.2015.01185.

Alessa, O., Ogura, Y., Fujitani, Y., Takami, H., Hayashi, T., Sahin, N., Tani, A., 2021. Comprehensive comparative genomics and phenotyping of *methylobacterium* species. Front. Microbiol. 12. https://doi.org/10.3389/fmicb.2021.740610.

Alleman, A.B., Stolyar, S., Marx, C.J., Leducq, J.-B., 2025. Led astray by 16S rRNA: phylogenomics reaffirms the monophyly of *Methylobacterium* and lack of support for *Methylorubrum* as a genus. ISME J. 19. https://doi.org/10.1093/ismejo/wraf011.

Ankenbrand, M.J., Keller, A., 2016. bcgTree: automatized phylogenetic tree building from bacterial core genomes. Genome 59, 783–791. https://doi.org/10.1139/gen-2015-0175.

Antipov, D., Hartwick, N., Shen, M., Raiko, M., Lapidus, A., Pevzner, P.A., 2016. plasmidSPAdes: assembling plasmids from whole genome sequencing data. Bioinformatics 32, 3380–3387. https://doi.org/10.1093/bioinformatics/btw493.

Bakker, P.A.H.M., Ran, L., Mercado-Blanco, J., 2014. Rhizobacterial salicylate production provokes headaches. Plant Soil 382, 1–16. https://doi.org/10.1007/s11104-014-2102-0.

Beauregard, P.B., Chai, Y., Vlamakis, H., Losick, R., Kolter, R., 2013. *Bacillus subtilis* biofilm induction by plant polysaccharides. Proc. Natl. Acad. Sci. 110. https://doi.org/10.1073/pnas.1218984110.

Begum, J.F., Tamilarasi, M., Pushpakanth, P., Balachandar, D., 2019. A simple method for direct isolation of N-acyl-L-homoserine lactone mediated biofilm-forming rhizobacteria from roots. J. Microbiol. Methods 156, 34–39. https://doi.org/10.1016/j.mimet.2018.11.018.

Bertelli, C., Laird, M.R., Williams, K.P., Lau, B.Y., Hoad, G., Winsor, G.L., Brinkman, F.S., 2017. IslandViewer 4: expanded prediction of genomic islands for larger-scale datasets. Nucleic Acids Res. 45, W30–W35. https://doi.org/10.1093/nar/gkx343.

Bijlani, S., Singh, N.K., Eedara, V.V.R., Podile, A.R., Mason, C.E., Wang, C.C.C., Venkateswaran, K., 2021. *Methylobacterium ajmalii* sp. Nov., isolated from the international space station. Front. Microbiol. 12. https://doi.org/10.3389/fmicb.2021.639396.

Carattoli, A., Zankari, E., García-Fernández, A., Voldby Larsen, M., Lund, O., Villa, L., Møller Aarestrup, F., Hasman, H., 2014. In silico detection and typing of plasmids using PlasmidFinder and plasmid multilocus sequence typing. Antimicrob. Agents Chemother. 58, 3895–3903. https://doi.org/10.1128/aac.02412-14.

Caten, C.E., Jinks, J.L., 1968. Spontaneous variability of single isolates of *Phytophthora infestans*. I. Cultural variation. Can. J. Bot. 46, 329–348.

Chanratana, M., Han, G.H., Roy Choudhury, A., Sundaram, S., Halim, Md.A., Krishnamoorthy, R., Kang, Y., Sa, T., 2017. Assessment of *Methylobacterium oryzae* CBMB20 aggregates for salt tolerance and plant growth promoting characteristics for bio-inoculant development. AMB Express 7. https://doi.org/10.1186/s13568-017-0518-7.

Chen, L.-B., OuYang, Y.-T., Liu, L., Jin, P.-J., Huang, R.-R., Pan, W.-Y., Wang, Y., Xing, J.-Y., She, T.-T., Jiao, J.-Y., Wang, S., Li, W.-J., 2024. *Methylobacterium nigriterrae* sp. Nov., isolated from black soil. Antonie Leeuwenhoek 117. https://doi.org/10.1007/s10482-024-01981-x.

Chistoserdova, L., Kalyuzhnaya, M.G., Lidstrom, M.E., 2009. The expanding world of methylotrophic metabolism. Annu. Rev. Microbiol. 63, 477–499. https://doi.org/10.1146/annurev.micro.091208.073600.

Danhorn, T., Fuqua, C., 2007. Biofilm Formation by plant-associated bacteria. Annu. Rev. Microbiol. 61, 401–422. https://doi.org/10.1146/annurev.micro.61.080706.093316.

Díaz Herrera, S., Grossi, C., Zawoznik, M., Groppa, M.D., 2016. Wheat seeds harbour bacterial endophytes with potential as plant growth promoters and biocontrol agents of *Fusarium graminearum*. Microbiol. Res. 186–187, 37–43. https://doi.org/10.1016/j.micres.2016.03.002.

Dworkin, M., Foster, J.W., 1958. Experiments with some microorganisms which utilize ethane and hydrogen. J. Bacteriol. 75, 592–603. https://doi.org/10.1128/jb.75.5.592-603.1958.

Fall, R., Benson, A.A., 1996. Leaf methanol — the simplest natural product from plants. Trends Plant Sci. 1, 296–301. https://doi.org/10.1016/s1360-1385(96)88175-0.

Gao, N., Fang, T., Liang, Y., Li, J., Zhao, X., Lu, W., 2024. *Methylobacterium flocculans* sp. Nov., a floc-forming bacterium isolated from aquaculture ponds. Curr. Microbiol. 81. https://doi.org/10.1007/s00284-024-03912-5.

Gao, R., Li, J., Li, H., Xie, X., Feng, G.-D., Zhu, H., 2025. *Methylobacterium litchii* sp. Nov., *Methylobacterium guangdongense* sp. Nov. and *Methylorubrum subtropicum* sp. Nov., isolated from the phyllosphere of litchi. Int. J. Syst. Evol. Microbiol. 75. https://doi.org/10.1099/ijsem.0.006639.

Golysheva, A.A., Litvinenko, L.V., Ivshina, I.B., 2025. Diversity of mercury-tolerant microorganisms. Microorganisms 13, 1350. https://doi.org/10.3390/microorganisms13061350.

Good, N.M., Vu, H.N., Suriano, C.J., Subuyuj, G.A., Skovran, E., Martinez-Gomez, N.C., 2016. Pyrroloquinoline quinone ethanol dehydrogenase in *Methylobacterium extorquens* AM1 extends lanthanide-dependent metabolism to multicarbon substrates. J. Bacteriol. 198, 3109–3118. https://doi.org/10.1128/jb.00478-16.

Green, P.N., Ardley, J.K., 2018. Review of the genus *Methylobacterium* and closely related organisms: a proposal that some *Methylobacterium* species be reclassified into a new genus, *Methylorubrum* gen. nov. Int. J. Syst. Evol. Microbiol. 68, 2727–2748. https://doi.org/10.1099/ijsem.0.002856.

Grossi, C.E.M., Fantino, E., Serral, F., Zawoznik, M.S., Fernandez Do Porto, D.A., Ulloa, R.M., 2020. *Methylobacterium* sp. 2A is a plant growth-promoting rhizobacteria that has the potential to improve potato crop yield under adverse conditions. Front. Plant Sci. 11. https://doi.org/10.3389/fpls.2020.00071.

Grossi, C.E.M., Tani, A., Mori, I.C., Matsuura, T., Ulloa, R.M., 2024. Plant growth-promoting abilities of *Methylobacterium* sp. 2A involve auxin-mediated regulation of the root architecture. Plant Cell Environ. 47, 5343–5357. https://doi.org/10.1111/pce.15116.

Grossi, C.E.M., Ulloa, R.M., Sahin, N., Tani, A., 2025. *Methylobacterium* as a key symbiont in plant-microbe interactions: its ecological and agricultural significance. Plant Biotechnol. 42, 229–241. https://doi.org/10.5511/plantbiotechnology.25.0309a.

Herigstad, B., Hamilton, M., Heersink, J., 2001. How to optimize the drop plate method for enumerating bacteria. J. Microbiol. Methods 44, 121–129. https://doi.org/10.1016/s0167-7012(00)00241-4.

Hoang, D.T., Chernomor, O., von Haeseler, A., Minh, B.Q., Vinh, L.S., 2017. UFBoot2: improving the ultrafast bootstrap approximation. Mol. Biol. Evol. 35, 518–522. https://doi.org/10.1093/molbev/msx281.

Huang, J., Yu, Z., Groom, J., Cheng, J.-F., Tarver, A., Yoshikuni, Y., Chistoserdova, L., 2019. Rare earth element alcohol dehydrogenases widely occur among globally distributed, numerically abundant and environmentally important microbes. ISME J. 13, 2005–2017. https://doi.org/10.1038/s41396-019-0414-z.

Huang, J.J., Han, J.-I., Zhang, L.-H., Leadbetter, J.R., 2003. Utilization of acyl-homoserine lactone quorum signals for growth by a soil pseudomonad and *Pseudomonas aeruginosa* PAO1. Appl. Environ. Microbiol. 69, 5941–5949. https://doi.org/10.1128/aem.69.10.5941-5949.2003.

Jiang, H.-Y., Liu, G.-H., Xu, Y.-J., Shen, H.-C., Gao, P., Zhou, S.-G., 2026. *Methylobacterium endophyticum* sp. Nov. and *Endoryza foliicola* gen. nov., sp. Nov., two novel endophytic bacterial species isolated from rice phyllosphere. Int. J. Syst. Evol. Microbiol. 76. https://doi.org/10.1099/ijsem.0.007090.

Kalyaanamoorthy, S., Minh, B.Q., Wong, T.K.F., von Haeseler, A., Jermiin, L.S., 2017. ModelFinder: fast model selection for accurate phylogenetic estimates. Nat. Methods 14, 587–589. https://doi.org/10.1038/nmeth.4285.

Knief, C., Ramette, A., Frances, L., Alonso-Blanco, C., Vorholt, J.A., 2010. Site and plant species are important determinants of the *Methylobacterium* community composition in the plant phyllosphere. ISME J. 4, 719–728. https://doi.org/10.1038/ismej.2010.9.

Kwak, M.-J., Jeong, H., Madhaiyan, M., Lee, Y., Sa, T.-M., Oh, T.K., Kim, J.F., 2014. Genome information of *Methylobacterium oryzae*, a plant-probiotic methylotroph in the phyllosphere. PLoS One 9, e106704. https://doi.org/10.1371/journal.pone.0106704.

Leducq, J.-B., Sneddon, D., Santos, M., Condrain-Morel, D., Bourret, G., Martinez-Gomez, N.C., Lee, J.A., Foster, J.A., Stolyar, S., Shapiro, B.J., Kembel, S.W., Sullivan, J.M., Marx, C.J., 2022. Comprehensive phylogenomics of *methylobacterium* reveals four evolutionary distinct groups and underappreciated phyllosphere diversity. Genome Biol. Evol. 14. https://doi.org/10.1093/gbe/evac123.

Liu, L., Zhang, S.-Y., Gao, P., Shen, H.-C., Rensing, C., Liu, G.-H., Zhou, S.-G., 2025. *Methylobacterium oryzisoli* sp. Nov., a novel methylotrophic methanol-utilizing bacterium isolated from the paddy soil. Int. J. Syst. Evol. Microbiol. 75. https://doi.org/10.1099/ijsem.0.006805.

Madhaiyan, M., Poonguzhali, S., 2014. *Methylobacterium pseudosasicola* sp. Nov. and *Methylobacterium phyllostachyos* sp. Nov., isolated from bamboo leaf surfaces. Int. J. Syst. Evol. Microbiol. 64, 2376–2384. https://doi.org/10.1099/ijs.0.057232-0.

Madhaiyan, M., Poonguzhali, S., Kang, B.-G., Lee, Y.-J., Chung, J.-B., Sa, T.-M., 2009. Effect of co-inoculation of methylotrophic *Methylobacterium oryzae* with *Azospirillum brasilense* and *Burkholderia pyrrocinia* on the growth and nutrient uptake of tomato, red pepper and rice. Plant Soil 328, 71–82. https://doi.org/10.1007/s11104-009-0083-1.

Masuda, S., Suzuki, Y., Fujitani, Y., Mitsui, R., Nakagawa, T., Shintani, M., Tani, A., 2018. Lanthanide-dependent regulation of methylotrophy in *Methylobacterium aquaticum* strain 22A. mSphere 3. https://doi.org/10.1128/msphere.00462-17.

Meier-Kolthoff, J.P., Auch, A.F., Klenk, H.-P., Göker, M., 2013. Genome sequence-based species delimitation with confidence intervals and improved distance functions. BMC Bioinf. 14. https://doi.org/10.1186/1471-2105-14-60.

Meneses, C.H.S.G., Rouws, L.F.M., Simões-Araújo, J.L., Vidal, M.S., Baldani, J.I., 2011. Exopolysaccharide production is required for biofilm formation and plant colonization by the nitrogen-fixing Endophyte *Gluconacetobacter diazotrophicus*. Mol. Plant Microbe Interact. 24, 1448–1458. https://doi.org/10.1094/mpmi-05-11-0127.

Mező, E., Hartmann-Balogh, F., Madarászné Horváth, I., Bufa, A., Marosvölgyi, T., Kocsis, B., Makszin, L., 2022. Effect of culture conditions on fatty acid profiles of bacteria and lipopolysaccharides of the genus *Pseudomonas*—GC-MS analysis on ionic liquid-based column. Molecules 27, 6930. https://doi.org/10.3390/molecules27206930.

Minh, B.Q., Schmidt, H.A., Chernomor, O., Schrempf, D., Woodhams, M.D., von Haeseler, A., Lanfear, R., 2020. IQ-TREE 2: new models and efficient methods for phylogenetic inference in the genomic era. Mol. Biol. Evol. 37, 1530–1534. https://doi.org/10.1093/molbev/msaa015.

Morohoshi, T., Kato, M., Fukamachi, K., Kato, N., Ikeda, T., 2008. N-Acylhomoserine lactone regulates violacein production in *Chromobacterium violaceum* type strain

ATCC 12472. FEMS Microbiol. Lett. 279, 124–130. https://doi.org/10.1111/j.1574-6968.2007.01016.x.
Murashige, T., Skoog, F., 1962. A revised medium for rapid growth and bio assays with tobacco tissue cultures. Physiol. Plantarum 15, 473–497. https://doi.org/10.1111/j.1399-3054.1962.tb08052.x.
O'Toole, G.A., 2011. Microtiter dish biofilm formation assay. J. Vis. Exp. https://doi.org/10.3791/2437.
Ondov, B.D., Treangen, T.J., Melsted, P., Mallonee, A.B., Bergman, N.H., Koren, S., Phillippy, A.M., 2016. Mash: fast genome and metagenome distance estimation using MinHash. Genome Biol. 17, 132. https://doi.org/10.1186/s13059-016-0997-x.
Palberg, D., Kisiała, A., Jorge, G.L., Emery, R.J.N., 2022. A survey of *Methylobacterium* species and strains reveals widespread production and varying profiles of cytokinin phytohormones. BMC Microbiol. 22. https://doi.org/10.1186/s12866-022-02454-9.
Park, C., Jung, H.S., Park, S., Jeon, C.O., Park, W., 2020. Dominance of gas-eating, biofilm-forming *Methylobacterium* species in the evaporator cores of automobile air-conditioning systems. mSphere 5, e00761. https://doi.org/10.1128/mSphere.00761-19, 19.
Parks, D.H., Imelfort, M., Skennerton, C.T., Hugenholtz, P., Tyson, G.W., 2015. CheckM: assessing the quality of microbial genomes recovered from isolates, single cells, and metagenomes. Genome Res. 25, 1043–1055. https://doi.org/10.1101/gr.186072.114.
Parsek, M.R., Greenberg, E.P., 2000. Acyl-homoserine lactone quorum sensing in Gram-negative bacteria: a signaling mechanism involved in associations with higher organisms. Proc. Natl. Acad. Sci. 97, 8789–8793. https://doi.org/10.1073/pnas.97.16.8789.
Patt, T.E., Cole, G.C., Hanson, R.S., 1976. *Methylobacterium*, a new genus of facultatively methylotrophic bacteria. Int. J. Syst. Bacteriol. 26, 226–229. https://doi.org/10.1099/00207713-26-2-226.
Priya, M., Kumutha, K., Senthilkumar, M., 2019. Impact of bacterization of rhizobium and *Methylobacterium radiotolerans* on germination and survivability in groundnut seed. Int. J. Curr. Microbiol. Appl. Sci. 8, 394–405. https://doi.org/10.20546/ijcmas.2019.808.045.
Pruesse, E., Peplies, J., Glöckner, F.O., 2012. SINA: accurate high-throughput multiple sequence alignment of ribosomal RNA genes. Bioinformatics 28, 1823–1829. https://doi.org/10.1093/bioinformatics/bts252.
Richter, M., Rosselló-Móra, R., Oliver Glöckner, F., Peplies, J., 2015. JSpeciesWS: a web server for prokaryotic species circumscription based on pairwise genome comparison. Bioinformatics 32, 929–931. https://doi.org/10.1093/bioinformatics/btv681.
Rowe, N.J., Tunstall, J., Galbraith, L., Wilkinson, S.G., 2000. Lipid composition and taxonomy of *[Pseudomonas] echinoides*: transfer to the genus *Sphingomonas*. Microbiology 146, 3007–3012. https://doi.org/10.1099/00221287-146-11-3007.
Samanta, D., Rauniyar, S., Saxena, P., Sani, R.K., 2024. From genome to evolution: investigating type II methylotrophs using a pangenomic analysis. mSystems 9. https://doi.org/10.1128/msystems.00248-24.
Sasser, M., 2001. Identification of bacteria by gas chromatography of cellular fatty acids. In: Technical Note, vol.101. Microbial ID, Inc., Newark, DE, USA.
Seemann, T., 2014. Prokka: rapid prokaryotic genome annotation. Bioinformatics 30, 2068–2069. https://doi.org/10.1093/bioinformatics/btu153.
Skovran, E., Raghuraman, C., Martinez-Gomez, N.C., 2019. Lanthanides in methylotrophy. Curr. Issues Mol. Biol. 33, 101–116. https://doi.org/10.21775/cimb.033.101.
Smith, J.L., Fratamico, P.M., Yan, X., 2011. Eavesdropping by bacteria: the role of SdiA in *Escherichia coli* and *Salmonella enterica* Serovar Typhimurium quorum sensing. Foodb. Pathog. Dis. 8, 169–178. https://doi.org/10.1089/fpd.2010.0651.
Sone, Y., Mochizuki, Y., Koizawa, K., Nakamura, R., Pan-Hou, H., Itoh, T., Kiyono, M., 2013. Mercurial-resistance determinants in *Pseudomonas* strain K-62 plasmid pMR68. AMB Express 3. https://doi.org/10.1186/2191-0855-3-41.
Spaepen, S., Vanderleyden, J., 2010. Auxin and plant-microbe interactions. Cold Spring Harbor Perspect. Biol. 3. https://doi.org/10.1101/cshperspect.a001438 a001438–a001438.
Stevenson, K., McVey, A.F., Clark, I.B.N., Swain, P.S., Pilizota, T., 2016. General calibration of microbial growth in microplate readers. Sci. Rep. 6, 38828. https://doi.org/10.1038/srep38828.
Swift, S., Allan Downie, J., Whitehead, N.A., Barnard, A.M.L., Salmond, G.P.C., Williams, P., 2001. Quorum sensing as a population-density-dependent determinant of bacterial physiology. Adv. Microb. Physiol. 45, 199–270. https://doi.org/10.1016/S0065-2911(01)45005-3.
Sy, A., Timmers, A.C.J., Knief, C., Vorholt, J.A., 2005. Methylotrophic metabolism is advantageous for *Methylobacterium extorquens* during colonization of *Medicago truncatula* under competitive conditions. Appl. Environ. Microbiol. 71, 7245–7252. https://doi.org/10.1128/aem.71.11.7245-7252.2005.
Tang, J., Li, Y., Zhang, L., Mu, J., Jiang, Y., Fu, H., Zhang, Y., Cui, H., Yu, X., Ye, Z., 2023. Biosynthetic pathways and functions of Indole-3-Acetic acid in microorganisms. Microorganisms 11, 2077. https://doi.org/10.3390/microorganisms11082077.
Tani, A., Mitsui, R., Nakagawa, T., 2021. Discovery of lanthanide-dependent methylotrophy and screening methods for lanthanide-dependent methylotrophs. Methods Enzymol. 650, 1–18.
Tatusova, T., DiCuccio, M., Badretdin, A., Chetvernin, V., Nawrocki, E.P., Zaslavsky, L., Lomsadze, A., Pruitt, K.D., Borodovsky, M., Ostell, J., 2016. NCBI prokaryotic genome annotation pipeline. Nucleic Acids Res. 44, 6614–6624. https://doi.org/10.1093/nar/gkw569.
Tsukahara, K., Sawada, H., Kohno, Y., Matsuura, T., Mori, I.C., Terao, T., Ioki, M., Tamaoki, M., 2015. Ozone-induced rice grain yield loss is triggered via a change in panicle morphology that is controlled by ABERRANT PANICLE ORGANIZATION 1 gene. PLoS One 10, e0123308. https://doi.org/10.1371/journal.pone.0123308.
Velmourougane, K., Prasanna, R., Saxena, A.K., 2017. Agriculturally important microbial biofilms: present status and future prospects. J. Basic Microbiol. 57, 548–573. https://doi.org/10.1002/jobm.201700046.
Vijayanand, N., Subramanian, S.R., Ponnerulan, B., Saminathan, E., Veerenan, U., Kathiresan, D., Subramani, N., 2021. Potential of pink pigmented methylotrophic bacteria on growth and physiology of cluster bean and soil microbial community. Biocatal. Agric. Biotechnol. 37, 102161. https://doi.org/10.1016/j.bcab.2021.102161.
Yoon, J.P., Kim, T.H., Park, S.Y., Yoon, K.Y., Kim, H.M., 2025. *Methylobacterium alsaeris* sp. Nov. and *Methylobacterium carpenticola* sp. Nov., isolated from a car air conditioning system. Int. J. Syst. Evol. Microbiol. 75. https://doi.org/10.1099/ijsem.0.006884.
Yu, Y.U., Lee, S.H., Jeon, C.O., Kim, K.H., 2026. *Methylobacterium synurae* sp. Nov., isolated from a freshwater alga *Synura petersenii*. Int. J. Syst. Evol. Microbiol. 76. https://doi.org/10.1099/ijsem.0.007077.
Zhang, S., Luo, Y., Zhang, K., Song, Z., Ling, L., Yu, X., Sun, Y., Li, J., Xiang, W., Wang, X., Zhao, J., 2024. *Methylobacterium amylolyticum* sp. Nov. and *Methylobacterium ligniniphilum* sp. Nov., isolated from soil. Int. J. Syst. Evol. Microbiol. 74. https://doi.org/10.1099/ijsem.0.006457.